RESEARCH MEMORANDUM

THE EFFECTS OF CAMBER AND TWIST ON THE AERODYNAMIC LOADING AND STALLING CHARACTERISTICS OF A LARGE-SCALE 45° SWEPT-BACK WING

By Lynn W. Hunton and Joseph K. Dew

Ames Aeronautical Laboratory
Moffett Field, Calif.

NATIONAL ADVISORY COMMITTEE
FOR AERONAUTICS

WASHINGTON
January 24, 1951

NATIONAL ADVISORY COMMITTEE FOR AERONAUTICS

RESEARCH MEMORANDUM

THE EFFECTS OF CAMBER AND TWIST ON THE AERODYNAMIC LOADING AND STALLING CHARACTERISTICS OF A LARGE-SCALE 45° SWEPT-BACK WING

By Lynn W. Hunton and Joseph K. Dew

SUMMARY

Pressure-distribution measurements have been obtained on two large-scale semispan wing-fuselage models having 45° of sweepback, an aspect ratio of 6, a taper ratio of 0.5, and 10-percent-thick sections normal to the quarter-chord line. One wing model had no camber and no twist and the other was cambered and twisted for approximately elliptic loading at a lift coefficient of 0.4. The investigation was conducted at a Reynolds number of 8 million and a Mach number of 0.2. Spanwise distribution of local lift coefficient, local center of pressure, and stalling characteristics of the wings are derived from the pressure data. Predicted characteristics from the Weissinger theory are compared with the experimental results.

The camber and twist significantly improved the upper surface loading of the wing at a lift coefficient of 0.4 through a reduction in the peak negative pressure coefficient from a value of −2.4 to −0.5. In the upper lift range, the onset of leading-edge separation on the wing was delayed from a lift coefficient of 0.65 to 1.09. Above a lift coefficient of 0.8, the instability of the wing was reduced but not eliminated by camber and twist.

An analysis of the pressure data for both of the swept wings and for comparable sections tested two-dimensionally showed that the stalling behavior of the outboard sections of each wing closely resembled that of the two-dimensional section. Hence, it was deduced that the stalling characteristics of the outboard sections of these swept-back wings were not greatly affected by the spanwise flow of the boundary-layer air.

The basic and additional span loadings computed by the Weissinger method showed generally good agreement with the experimental data at

moderate lift coefficients. At the higher lift coefficients the agreement became less satisfactory as the experimental spanwise center of load moved inboard.

INTRODUCTION

Theoretical studies of the load distribution on swept-back wings, for subsonic flow (reference 1) as well as for supersonic flow (reference 2), have shown that significant improvements in the cruising or high-speed performance of highly swept-back wings could be achieved through the use of camber and twist. Similarly, from a low-speed standpoint, such camber and twist appeared advantageous as a means of alleviating some of the landing deficiencies of high-speed plan forms. In order to examine and evaluate the low-speed advantages of camber and twist, two 45° swept-back wings of aspect ratio 6, one cambered and twisted (as described in reference 3) for a lift coefficient of 0.4 and the other uncambered and untwisted, were tested. Force test and tuft-study results obtained at a Reynolds number of 8 million and a Mach number of 0.2 were reported in reference 3. Since over-all force characteristics and tuft data are inadequate for purposes of a detailed study of the flow on a wing, extensive pressure-distribution data were also obtained and are the subject of this report. Included herein with the pressure data are the loading characteristics across the span as determined from integrations of the pressure data.

NOTATION

The semispan-wing data are presented in the form of standard NACA coefficients and symbols which are applicable to a full-span configuration. Moments are referred to the quarter point of the mean aerodynamic chord (see fig. 1), and all coefficients are based on the dimensions and area[1] of the untwisted wing.

C_L lift coefficient $\left(\frac{L}{qS}\right)$

$C_{L_{max}}$ maximum lift coefficient

[1]The projected area of the cambered, twisted wing at 0° angle of attack of the wing-root section was approximately 0.5 percent less than the area of the untwisted wing.

C_D drag coefficient $\left(\frac{D}{qS}\right)$

C_m pitching-moment coefficient $\left(\frac{M}{qS\bar{c}}\right)$

P pressure coefficient $\left(\frac{p_l - p_o}{q}\right)$

c_l local lift coefficient $\left(\frac{\text{local lift}}{qc}\right)$

c_m local pitching-moment coefficient referred to c/4 $\left(\frac{\text{local pitching moment}}{qc^2}\right)$

D drag on semispan wing

L lift on semispan wing

M pitching moment on semispan wing

R Reynolds number based on $\bar{c}$

S area of semispan wing, square feet

b span of complete wing, feet

c local chord measured parallel to plane of symmetry, feet

$\bar{c}$ wing mean aerodynamic chord $\left(\frac{\int_o^{b/2} c^2\,dy}{\int_o^{b/2} c\,dy}\right)$, feet

q free-stream dynamic pressure, pounds per square foot

p_o free-stream static pressure, pounds per square foot

p_l local static pressure, pounds per square foot

x distance from leading edge along chord line measured parallel to plane of symmetry, feet

y perpendicular distance from plane of symmetry along semispan, feet

α angle of attack of wing root section, degrees

ϵ angle of twist with respect to root chord (positive for washin), degrees

η fraction of semispan $\left(\frac{2y}{b}\right)$

MODEL AND APPARATUS

The principle dimensions of the two semispan wing–fuselage models used in this investigation are shown in figure 1. The tunnel floor served as a reflection plane, and the models were supported on a turntable fixed to the wind-tunnel six-component balance system. A view of the semispan test installation is shown in figure 2.

Except for camber and twist, the two wing–fuselage models were identical, having 45° of sweepback of the quarter-chord line, an aspect ratio of 6, and a taper ratio of 0.5. The uncambered, untwisted wing had the NACA 64A010 section normal to the quarter-chord line. The cambered, twisted wing had the NACA 64A810, a = 0.8 (modified as shown in reference 4) section normal to the quarter-chord line (coordinates given in table I). This wing was twisted to provide 10° washout (streamwise) at the tip, as shown in figure 3. The quarter-chord line was used as the axis about which the sections normal to quarter-chord line were twisted. The surface contour of the wing was then generated by straight-line elements between equal percent-chord points of the sections. The tips of the wings were formed by a half body having a radius equal to the corresponding half thickness of the tip section.

The fuselage consisted of half a body of revolution with a fineness ratio of 4.9. As shown in figure 1, the midsection was cylindrical with a 2.5-foot radius while the nose and tail fairing contour was generated by an arc with a radius of 12 feet. The wing incidence for both wing–body combinations was zero, based on the angle of attack of the wing-root-section chord line with respect to the longitudinal axis of the fuselage.

Each wing was equipped with 240 static-pressure orifices equally divided among six spanwise stations and distributed streamwise, as shown in figure 3.

TESTS AND CORRECTIONS

Measurements of pressure distribution were made on both models through an angle-of-attack range from 0° to the angle for $C_{L_{max}}$. These data were obtained at a Reynolds number of 8 million based on the mean aerodynamic chord of 6.21 feet. This Reynolds number corresponds to a dynamic pressure of about 55 pounds per square foot and a Mach number of 0.2.

The angle-of-attack data were corrected for tunnel-wall effects by the addition of the following correction which was derived from reference 5 for an unswept-semispan-wing installation:

$$\Delta\alpha = 0.26\ C_L$$

RESULTS AND DISCUSSION

The pressure-distribution investigation was undertaken on these wings for the purpose of showing the effect of camber and twist on the aerodynamic loading and to provide a means by which the stalling behavior of the wings could be analyzed. The aerodynamic loading of both wings is indicated by the results presented in figures 4 and 5, and the stalling characteristics of the two wings are described with the aid of the results presented in figures 6 to 9. The basic pressure data for the six rows of pressure orifices for each wing at angles of attack ranging from 0° to the angle for stall, from which the aforementioned results were derived, are presented in figures 10 and 11.

Loading Characteristics

Spanwise distribution of local lift coefficient.- In figure 4 is given the spanwise variation of local lift coefficient c_l for the uncambered, untwisted wing (hereinafter called the plain wing), and the cambered, twisted wing. The curves, derived from the integration of the areas under the pressure diagrams of figures 10 and 11, were determined for angles of attack[2] corresponding to lift coefficients of the plain wing of 0.2, 0.4, 0.6, and 0.8 and to lift coefficients of the cambered, twisted wing of 0, 0.2, 0.4, 0.6, 0.8, and 1.07. To illustrate

[2]The appropriate angles of attack for the various lift coefficients were determined from the lift curves of the wings measured from force tests. Such a procedure for correlating the measured span loading with wing C_L was made necessary by the lack of pressure data over the root areas of the two models. This lack prevented a determination of total lift from pressure distribution.

the degree of accuracy of the Weissinger simplified lifting-surface theory for predicting the span loading (discussed in reference 6), the theoretical c_l distribution computed by this method for each of the afore-mentioned values of wing lift coefficient are shown in the figures for each wing along with the experimental data. In making such a correlation it is necessary to assume, of course, that the presence of the fuselage exerted a negligible effect on the over-all spanwise distribution of c_l. For the plain wing, it may be noted that the theory was satisfactory for predicting the spanwise distribution of c_l for wing lift coefficients ranging to 0.6 (which is about 0.6 $C_{L_{max}}$) at which point separation of flow near the tip occurred. For the cambered, twisted wing the theoretical c_l variation showed excellent agreement with the test data for lift coefficients of the wing of 0, 0.2, and 0.4 and satisfactory agreement for lift coefficients of 0.6 and 0.8.

At lift coefficients approaching $C_{L_{max}}$ for both wings, these comparisons show that the experimental loading gradually shifted inboard, resulting in a steady increase in departure of theory from experiment as lift increased.

On the plain wing, which had no twist, the spanwise loading consisted of only the additional type (that due to angle of attack); whereas on the cambered, twisted wing, the loading was made up of both the additional type and the basic type (that due to twist). The comparisons of the curves in figure 4 showing satisfactory agreement between theory and experiment for both wings, therefore, clearly demonstrate the reliability of the Weissinger method for predicting the basic as well as the additional types of loading on highly swept wings at moderate lift coefficients.

Surface pressures.- In figure 5 are shown plots of lines of constant pressure coefficient on the upper surfaces of each of the wings at several angles of attack. By comparing the pressure distributions of the two wings at approximately equal lift coefficients it may be noted that the camber and twist effected a significant reduction in the peak negative pressures through a more uniform distribution of the loading. At an angle of attack of 6.1°, corresponding closely to the design lift coefficient of 0.4 for the cambered, twisted wing, the improvement amounted to a reduction in the peak negative pressure coefficient from a value of the order of -2.4 to a value of -0.5.

Stalling Characteristics

The pressure-distribution data at the various stations on each wing, given in figures 10 and 11 for the plain wing and for the cambered, twisted wing, respectively, have been scrutinized in order to

define the stalling characteristics. For additional clarification of this stalling picture, figures 7 and 8 have also been prepared which show, respectively, the variation of local center of pressure and local pitching-moment coefficient with angle of attack and the variation of pressure coefficient with local lift coefficient.

Plain wing.- The static longitudinal stability of the plain wing, shown in figure 6(a), was nearly constant up to an angle of attack of 8° corresponding to a lift coefficient of about 0.48. At slightly higher lift coefficients, the wing exhibited a small increase in stability. A close examination of the center-of-pressure characteristics in figure 7 and the pressure data in figure 10 revealed no explanation for this small shift of the aerodynamic center. Thus, the necessary change in pressures apparently was not localized but was sufficiently distributed over the wing so that the magnitude of any local change fell within the accuracy of the pressure measurements.

Initial flow separation on the wing occurred near the tip at an angle of attack of about 11.5° (C_L of 0.65) and marked the beginning of an abrupt drag rise and instability of the wing pitching moments. This separation appeared to be associated with the formation of a bubble of separated flow near the leading edge (similar to that described in reference 7). Evidence of this laminar separation and reattachment of flow may be seen in figure 10(f) which shows, at an angle of attack of 12.2°, a partial collapse of the leading-edge peak pressure accompanied by the formation of a region of approximately constant pressure over the forward 15 percent of the chord. A number of two-dimensional tests of sections (e.g., references 7 and 8) have shown this type of separation to be a characteristic of thin sections having relatively small leading-edge radii. Above 13.5° angle of attack, the flow separation at the tip was complete with no reattachment of the flow to the surface behind the leading edge. With further increase in angle of attack, this flow separation spread gradually inboard until at $C_{L_{max}}$ of the wing of 0.94, corresponding to an angle of attack of 23°, the flow was detached over almost the entire upper surface.

The progression of the stall from the tip to the root was the basic cause of the unstable pitching moments of the wing in the upper lift range shown in figure 6(a). The local center-of-pressure and local pitching-moment-coefficient results in figure 7 illustrate this gradual stall progression by the variation in angle of attack at which an abrupt break in the curves occurred for the various stations across the span. As would be expected on the basis of two-dimensional section data, the resulting moment change of each section at stall was in the direction of increased stability; whereas the stability of the total wing, as noted earlier, decreased sharply with the occurrence of flow separation. This clearly demonstrates the dominant influence on the longitudinal stability of swept wings that changes in span loading have as compared to section-moment characteristics.

Cambered, twisted wing.- Local lift curves and wing force characteristics for the cambered, twisted wing are given in figure 6(b). For angles of attack of the wing below 1°, the pitching-moment-coefficient data indicate a position of the aerodynamic center of approximately $0.40\bar{c}$. The explanation for this rearward position of the aerodynamic center may be seen in the pressure data of figure 11(f) as resulting from separation on the lower surface of the wing tip near the leading edge. A similar lower-surface separation was described in reference 9 concerning results of two-dimensional tests of the NACA 64A810 section. It was indicated that the formation of a localized bubble of separated flow on the lower surface caused both an increase in negative lift and a strong positive trend of the section pitching moment.

For the angle-of-attack range from 1° to about 12° there appeared to be no separation of flow on the wing based on the force- and pressure-data results. Beginning with an angle of attack of about 12°, however, the wing pitching moments, wing lift-curve slope, and local lift-curve slopes all show evidence of changes in the flow. It is apparent from the local lift curves of figure 6(b) that the outboard area of the wing suffered losses in lift-curve slope; whereas the lift curves of inboard stations remained nearly linear up to the angle of attack for $C_{l_{max}}$ of the wing. An examination of the pressures indicates that the losses in lift-curve slope at outboard stations are attributable to flow separation near the trailing edge. In figure 8(b), showing the variation of the pressure coefficient P with c_l for an inboard station (0.167 semispan) and an outboard station (0.815 semispan), the convergence of the trailing-edge pressures toward a common value of P in the upper lift range at the outboard station is indicative of trailing-edge separation over this region of the wing. Evidence of this separation may also be seen in figure 7 where the variation of local pitching-moment coefficient with angle of attack for the various stations across the span shows an increasing degree of instability for each station in progressing from the root to the tip. Of further significance, regarding this stalling picture, are the results presented in reference 9 from two-dimensional tests of the NACA 64A810 section wherein it was observed that the section suffered a gradual loss in lift-curve slope and an unstable shift of the aerodynamic center as a result of the growth of turbulent separation near the trailing edge. The pressure variations for the two-dimensional section, derived from the data of this reference, have been included in figure 8(b) for comparison with the data measured on the wing. Even though the wing pressure data presented are for streamwise stations, the comparison is still valid since the distribution of the pressures along the chord is affected very little by a change from the streamwise direction to the direction normal to the quarter-chord line. The absolute values of P and c_l for the two- and the three-dimensional case, however, differ approximately by the $\cos^2 45°$ following the simple sweep concept. A comparison of the results in figure 8(b) shows that the pressure

variations for the 0.815-semispan station, indicating trailing-edge separation, closely resemble the pressure characteristics for the two-dimensional section. The data for the inboard station, on the other hand, show no such similarity with the two-dimensional data. The reduction in separation at this station thus accounts for the more linear slopes of the lift curves for the inboard area of the wing noted in figure 6(b).

To further illustrate these comparisons between the wing stations and the two-dimensional section, figure 9 has been prepared showing the ratio of the wing section pressure coefficient to the two-dimensional section pressure coefficient at the 0.8 chord point as a function of percent $c_{l_{max}}$. Curves for this ratio are given for both the inboard and the outboard stations on the wing. It may be noted that all values of P were divided by c_l in order that any difference in effective dynamic pressure between the two- and three-dimensional data could be neglected. For the same reason, percent $c_{l_{max}}$ has been used as the basis for matching the two-dimensional data to the three-dimensional section data. A value of unity for the ratio $(P/c_l)_{3-dim.}/(P/c_l)_{2-dim.}$ indicates perfect correlation. The curve for the outboard station may be seen to show good agreement with the two-dimensional data throughout the high-lift range thus indicating that the progression of turbulent separation in both cases was nearly identical. The curve for the inboard station, in contrast, deviates sharply from the line of perfect correlation in a direction which shows that the growth of P is maintained beyond the start of turbulent separation on the two-dimensional section. [Thus, it would appear that the stalling characteristics of the outboard sections[3] of the wing were essentially similar to those which would be expected from two-dimensional section characteristics and, hence, were not too greatly affected by the spanwise flow of the boundary-layer air.] The departure of the characteristics of the inboard stations from two-dimensional results is most likely attributable to a boundary-layer-control effect caused by the drainage of the boundary-layer air away from the inboard area of the wing. This is not surprising since it is known from two-dimensional investigations that the removal of boundary-layer air over the afterpart of a section by means of suction slots is very effective in preventing turbulent separation. In the case of thin sections with little or no camber where turbulent separation is negligible, such as on the plain wing, the effect of boundary-layer removal over the aft portions of the wing will be small. This may be seen in figure 8(a) where the variations of pressure coefficient with c_l for both the inboard and outboard stations (0.167 and 0.924 semispan, respectively) on the wing closely match the two-dimensional section[4] (NACA 64A010) characteristics up to the c_l

[3]A comparison of the pressure data for the 0.924-semispan station with the two-dimensional data showed the same similarity as that demonstrated by the 0.815-semispan station.

[4]Pressure data for the NACA 64A010 section given in figure 8(a) were derived from results of two-dimensional tests reported in reference 8.

(about 0.6) where initial leading-edge separation occurred at the wing tip. The inference to be drawn from these results, therefore, is that on swept-back wings, the use of an airfoil section which responds to boundary-layer control near the trailing edge (such as highly cambered sections of the uniform-load type) will lead to dissimilar section lift curves across the span. Inboard section lift curves will be nearly linear; whereas those for outboard sections will resemble the two-dimensional section characteristics and be rounded. This will entail a shift inboard of the spanwise center of load which, on a swept-back wing, will constitute one factor contributing to the forward movement of the aerodynamic center of the wing.

The drag characteristics, unlike the lift and moment results, exhibited little sign of the changes in flow occurring on the wing in the upper lift-coefficient range. Until $C_{L_{max}}$ was reached, the maintenance of leading-edge suction was sufficient to largely offset the pressure drag associated with the turbulent separation.

The $C_{L_{max}}$ of the cambered, twisted wing was 1.09 and was reached at an angle of attack of about 21° as shown in figure 6(b). The pressure data in figure 11 for this angle of attack show that although separation was present near the trailing edge of most of the stations the wing was free of any leading-edge separation. With an increase in angle of attack to 22.3° it may be seen that a large change in the pressures occurred as a result of flow separation near the leading edge at all stations outboard of the 0.167 semispan station. However, the type of separation at the leading edge was different for the inboard and the outboard stations. At the inboard stations (0.383 and 0.545 semispan), the data reveal evidence of a laminar separation and reattachment type of flow which resulted in a sharp increase in lift noted in figure 6(b). At the outboard stations (0.707, 0.815, and 0.924 semispan), it appears that turbulent separation progressed forward almost to the leading edge and caused a large loss in lift. Which of these two types of flow separation actually precipitated the final stall of the wing is not clear from these data.

Evaluation of tuft studies.- In reference 3 certain conclusions were drawn regarding the stalling characteristics of the plain and the cambered, twisted wing which were based on observations of tufts on the upper surfaces of the wings. With pressure data, however, a much more precise analysis is possible. On the cambered, twisted wing the tufts revealed only a spanwise flow of the boundary-layer air but no roughness or turbulence until $C_{L_{max}}$ was reached when separation of flow occurred near the leading edge. In the case of the plain wing the action of the tufts was the same, showing only a spanwise flow until the flow separated from the leading edge. However, from the pressure data it is known that for these two wings the flow conditions near the trailing edge just preceding the incidence of separation near the leading edge were quite dissimilar. As discussed in the preceding section

of this report, on the cambered, twisted wing there was turbulent separation leading to poor pressure recovery; whereas on the plain wing essentially no turbulent separation was present. Thus, it is apparent that tuft-study results are rather inconclusive for purposes of defining separation on a swept wing and are useful primarily as an indication of the direction of flow of the surface boundary-layer air and of the presence of flow separation near the leading edge.

CONCLUDING REMARKS

Cambering and twisting a 45° swept-back wing for a design lift coefficient of 0.4 resulted in a significant improvement in the upper-surface load distribution at this design lift coefficient. Further, in the upper lift-coefficient range, the onset of leading-edge separation and the attendant abrupt drag rise were delayed from a lift coefficient of about 0.65 to 1.09. The forward shift of the aerodynamic center in the upper lift-coefficient range was reduced but not eliminated by the camber and twist. The cause of the forward shift of the aerodynamic center, however, was completely changed. On the uncambered, untwisted wing it resulted from abrupt separation of flow from the leading edge; whereas, on the cambered, twisted wing, it resulted from a gradual spread, both chordwise and spanwise, of separation of flow from the wing trailing edge.

On the basis of a comparison of the pressures at an inboard and an outboard station on the cambered, twisted wing with the corresponding two-dimensional section pressure data, it was deduced that the spanwise flow of the boundary-layer air resulted in a favorable effect at the inboard sections of the wing and caused little or no effect at the outboard sections. Consequently, the linear range of the local lift curves for inboard sections was extended, while the lift curves for outboard sections resembled that of the two-dimensional section and were rounded. The analysis points to the conclusion that, on swept-back wings, the use of a highly cambered section for which the lift characteristics respond to boundary-layer control near the trailing edge will entail a gradual shift inboard of the center of load in the upper lift range and, consequently, a forward shift of the aerodynamic center.

Theoretical span loadings of either the additional or the basic types, computed by the Weissinger simplified lifting-surface theory, gave good to excellent agreement with experiment in the moderate lift

range. In the upper lift range the experimental spanwise center of load moved inboard.

Ames Aeronautical Laboratory,
National Advisory Committee for Aeronautics,
Moffett Field, Calif.

REFERENCES

1. Stevens, Victor I., Jr.: Theoretical Basic Span Loading Characteristics of Wings With Arbitrary Sweep, Aspect Ratio, and Taper Ratio. NACA TN 1772, 1948.

2. Jones, Robert T.: Estimated Lift-Drag Ratios at Supersonic Speed. NACA TN 1350, 1947.

3. Hunton, Lynn W.: Effects of Twist and Camber on the Low-Speed Characteristics of a Large-Scale 45° Swept-Back Wing. NACA RM A50A10, 1950.

4. Loftin, Laurence K., Jr.: Theoretical and Experimental Data for a Number of NACA 6A-Series Airfoil Sections. NACA TR 903, 1948.

5. Glauert, H.: The Elements of Aerofoil and Airscrew Theory. The Macmillan Company, N.Y., 1943.

6. DeYoung, John, and Harper, Charles W.: Theoretical Symmetric Span Loading at Subsonic Speeds for Wings Having Arbitrary Plan Form. NACA Rep. 921, 1948.

7. McCullough, George B., and Gault, Donald E.: Boundary-Layer and Stalling Characteristics of the NACA 64A006 Airfoil Section. NACA TN 1923, 1949.

8. Peterson, Robert F.: Boundary-Layer and Stall Characteristics of an NACA 64A010 Airfoil Section. NACA RM A50I22, 1950.

9. McCullough, George B., and Haire, William M.: Low-Speed Characteristics of Four Cambered, 10-Percent-Thick NACA Airfoil Sections. NACA TN 2177, 1950.

TABLE I.- COORDINATES OF THE AIRFOIL SECTIONS
[Stations and ordinates given in percent of airfoil chord.]

NACA 64A010	
Station	Ordinate
0	0
.5	.804
.75	.969
1.25	1.225
2.5	1.688
5	2.327
7.5	2.805
10	3.199
15	3.813
20	4.272
25	4.606
30	4.837
35	4.968
40	4.995
45	4.894
50	4.684
55	4.388
60	4.021
65	3.597
70	3.127
75	2.623
80	2.103
85	1.582
90	1.062
95	.541
100	.021
L.E. radius = 0.687	
T.E. radius = 0.023	

TABLE I.- CONCLUDED
[Stations and ordinates given in percent of airfoil chord.]

NACA 64A810 (a = 0.8 modified)			
Upper surface		Lower surface	
Station	Ordinate	Station	Ordinate
0	0	0	0
.214	.976	.785	−.526
.428	1.231	1.072	−.597
.881	1.650	1.619	−.686
2.064	2.475	2.936	−.787
4.506	3.716	5.494	−.832
6.984	4.703	8.016	−.811
9.479	5.541	10.521	−.771
14.500	6.902	15.500	−.658
19.543	7.968	20.457	−.526
24.601	8.795	25.399	−.383
29.668	9.420	30.332	−.232
34.742	9.857	35.258	−.065
39.820	10.107	40.180	.123
44.900	10.150	45.100	.364
49.977	10.005	50.023	.637
55.049	9.693	54.951	.917
60.114	9.225	59.886	1.187
65.169	8.612	64.831	1.426
70.215	7.850	69.785	1.610
75.252	6.932	74.748	1.710
80.300	5.819	79.700	1.657
85.292	4.441	84.708	1.331
90.204	3.004	89.796	.920
95.104	1.512	94.896	.450
100.000	.021	100.000	−.021
L.E. radius = 0.687 T.E. radius = 0.023			

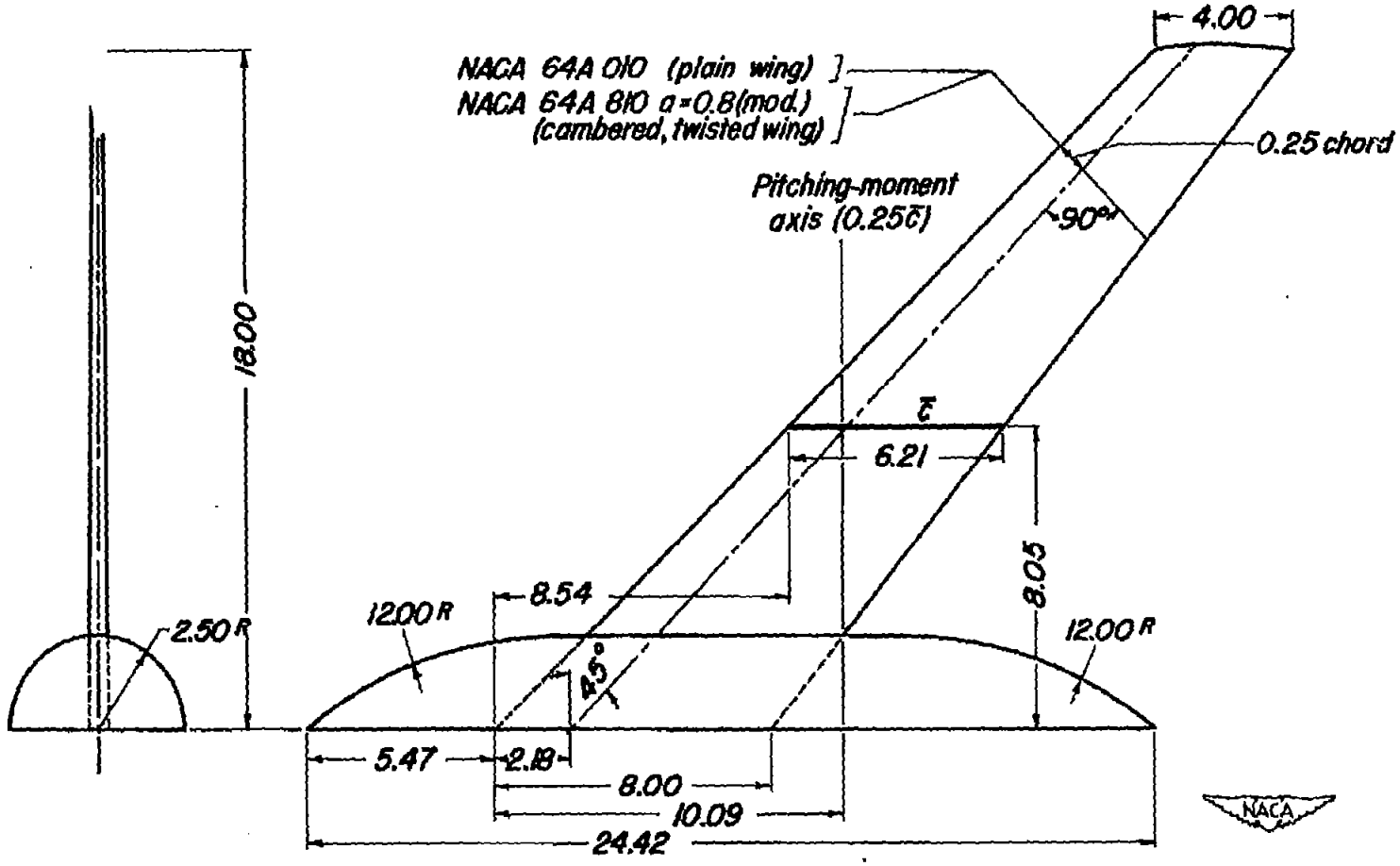

Note: All dimensions given in feet unless otherwise specified.

Figure 1.— Dimensions of the semispan models.

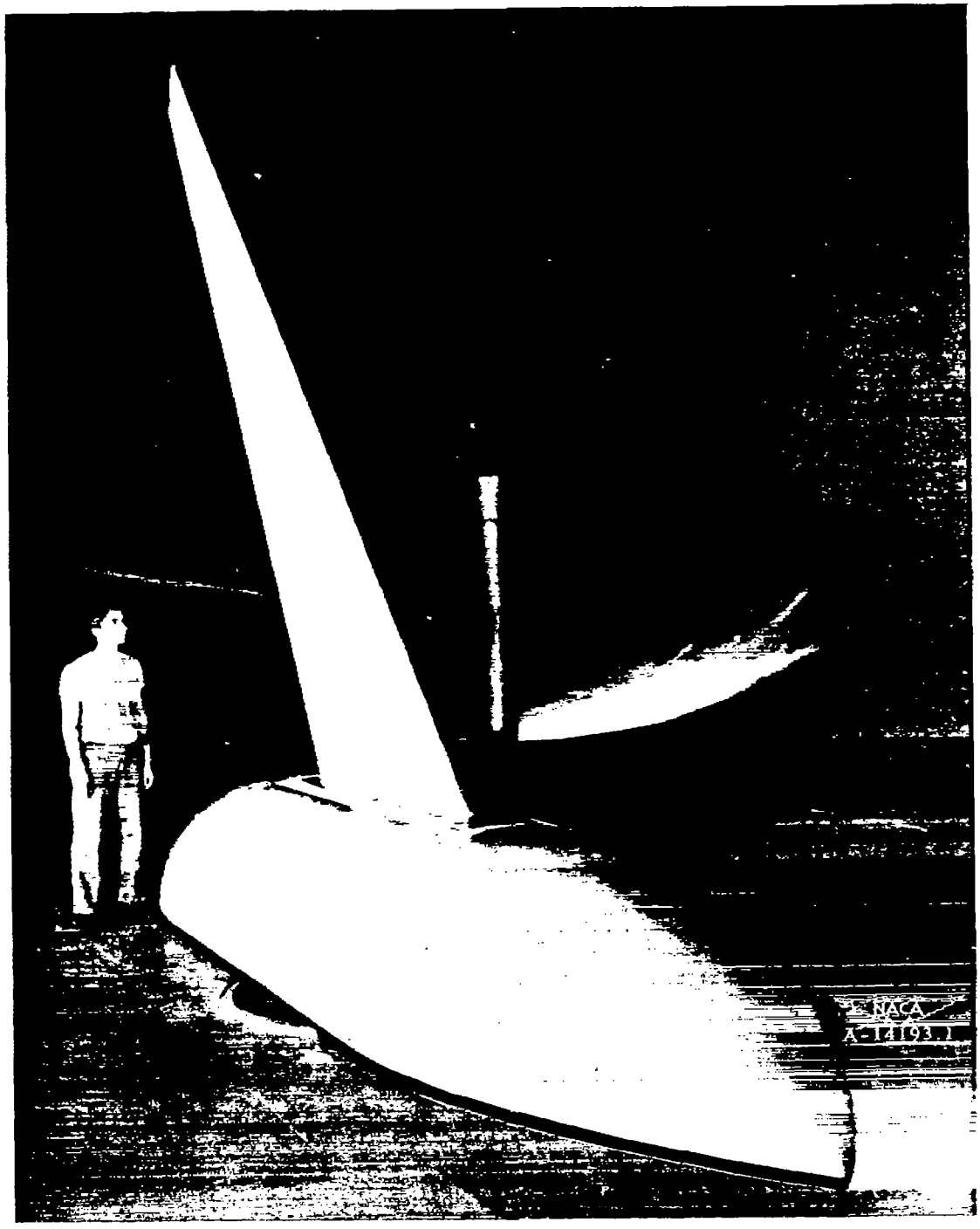

Figure 2.— Three-quarter front view of the cambered, twisted semispan wing-fuselage installation in the Ames 40- by 80-foot wind tunnel.

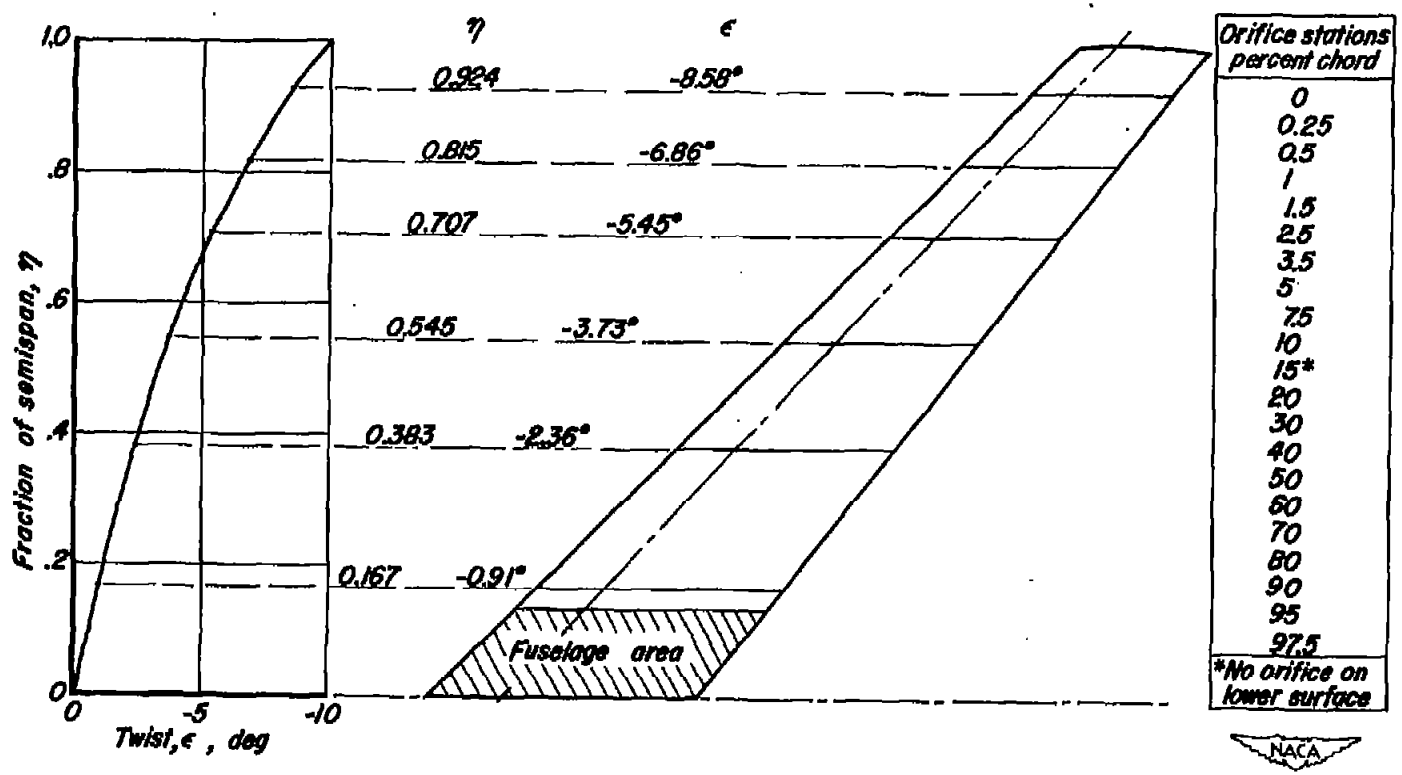

Figure 3.—The wing plan form showing the spanwise variation of twist and the location of the pressure orifice stations.

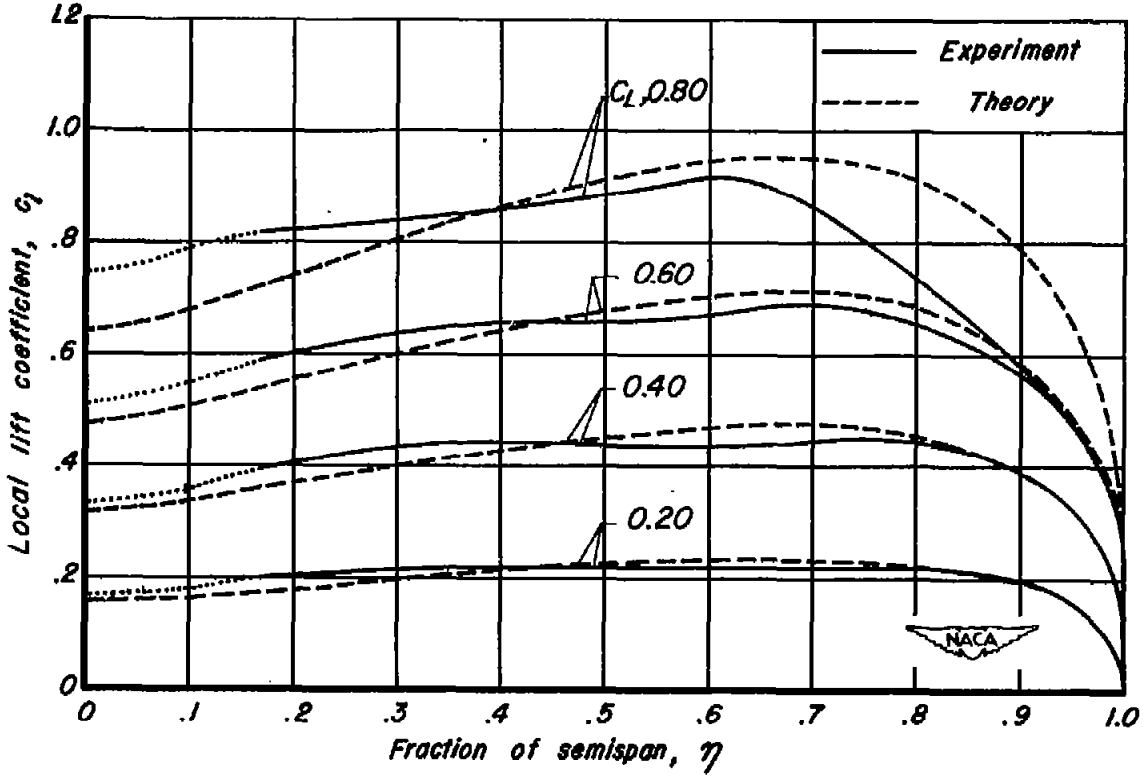

(a) Plain wing.

Figure 4.—Comparison of the theoretical and experimental spanwise distribution of local lift coefficient for several wing lift coefficients.

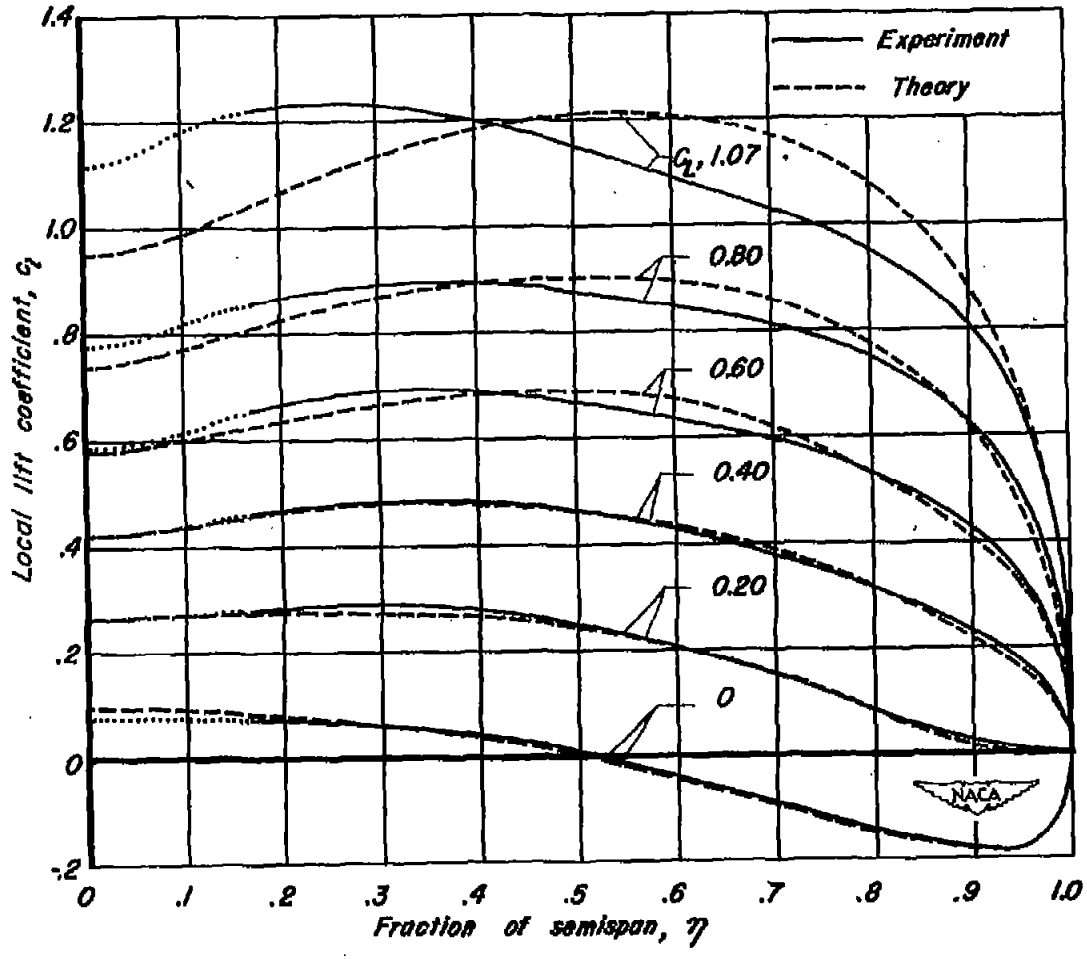

(b) Cambered, twisted wing.

Figure 4.– Concluded.

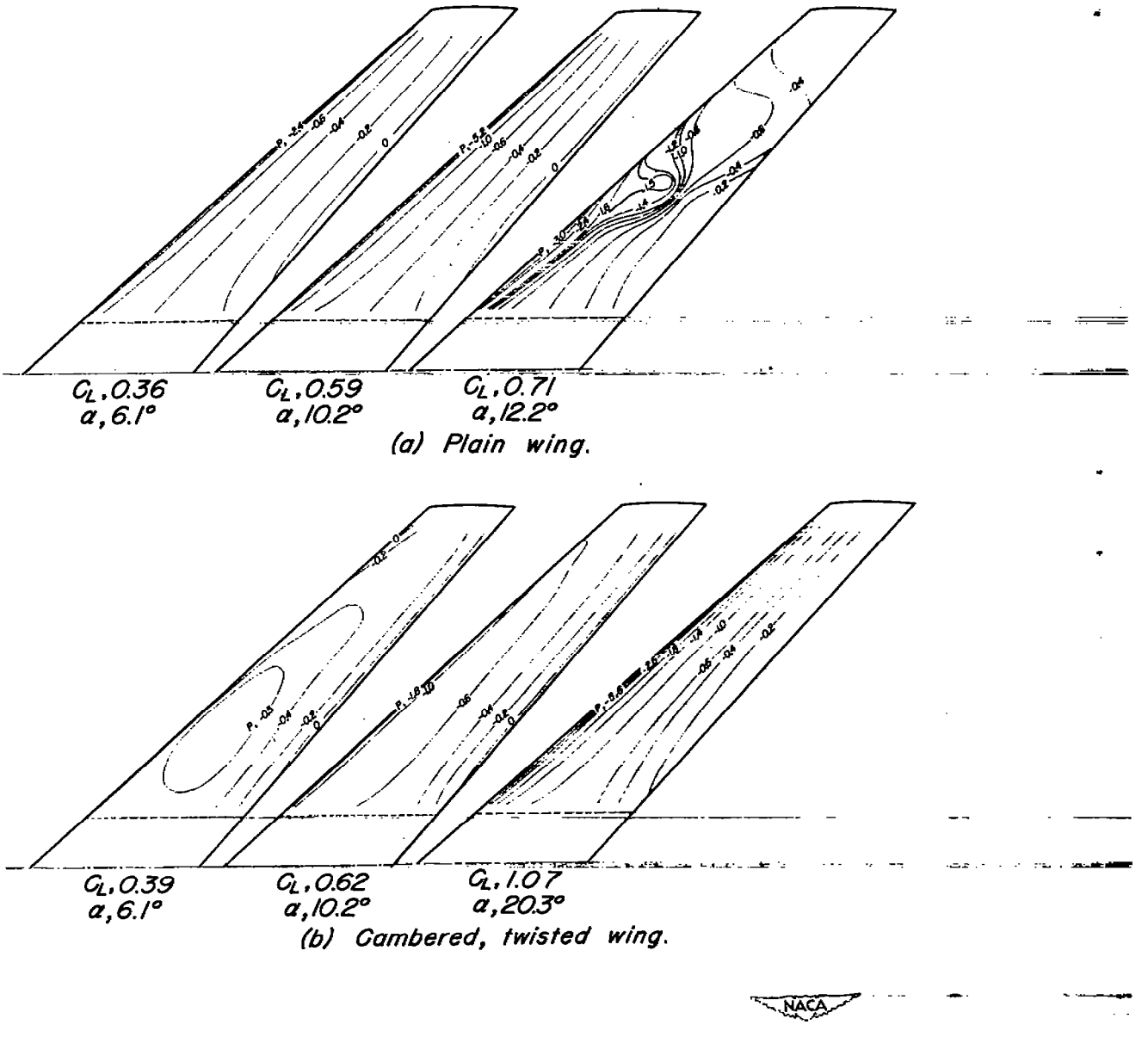

Figure 5.- Effect of camber and twist on the upper-surface pressure contours for several wing lift coefficients.

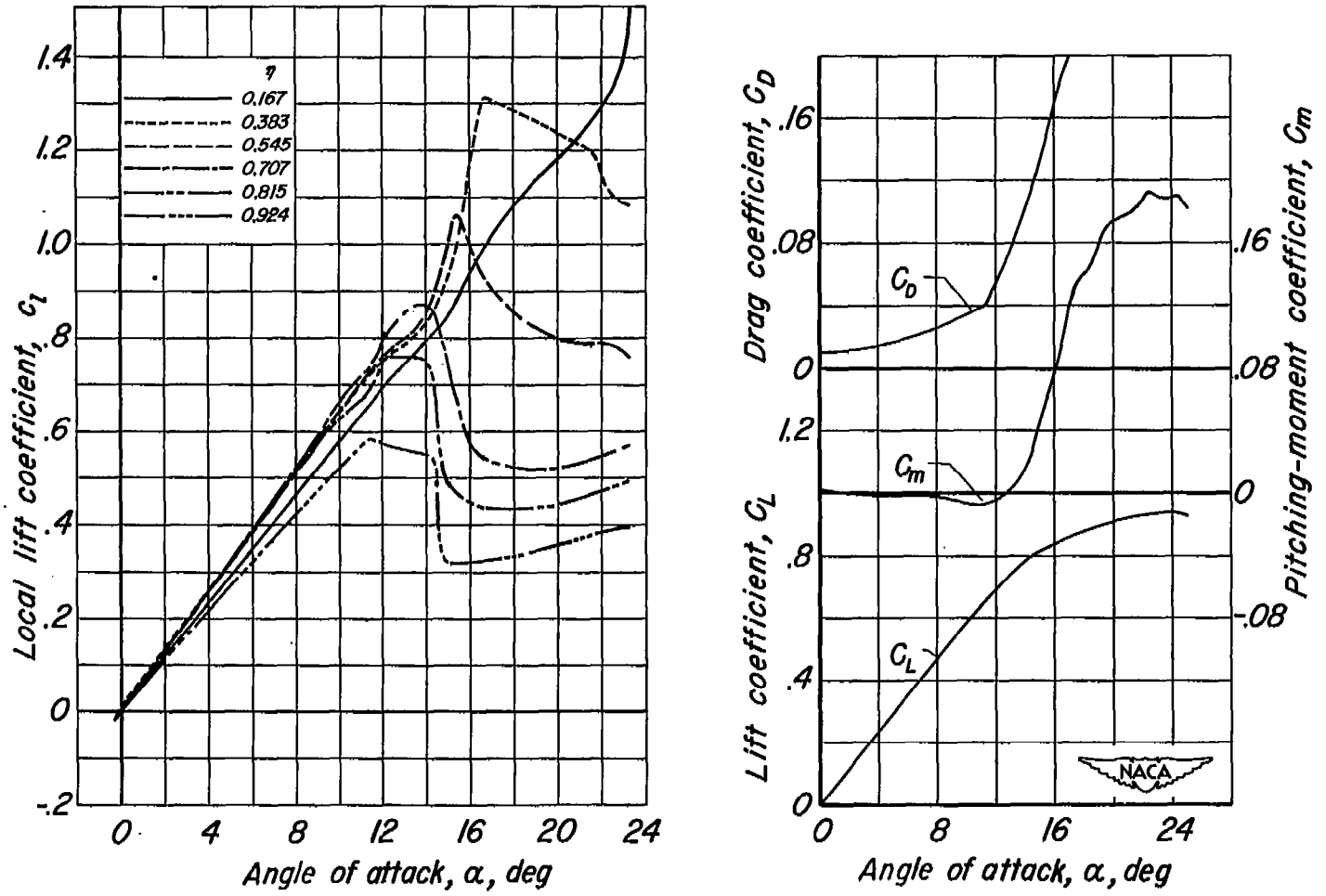

(a) Plain wing.

Figure 6.– Correlation of the local lift curves with the wing force characteristics.

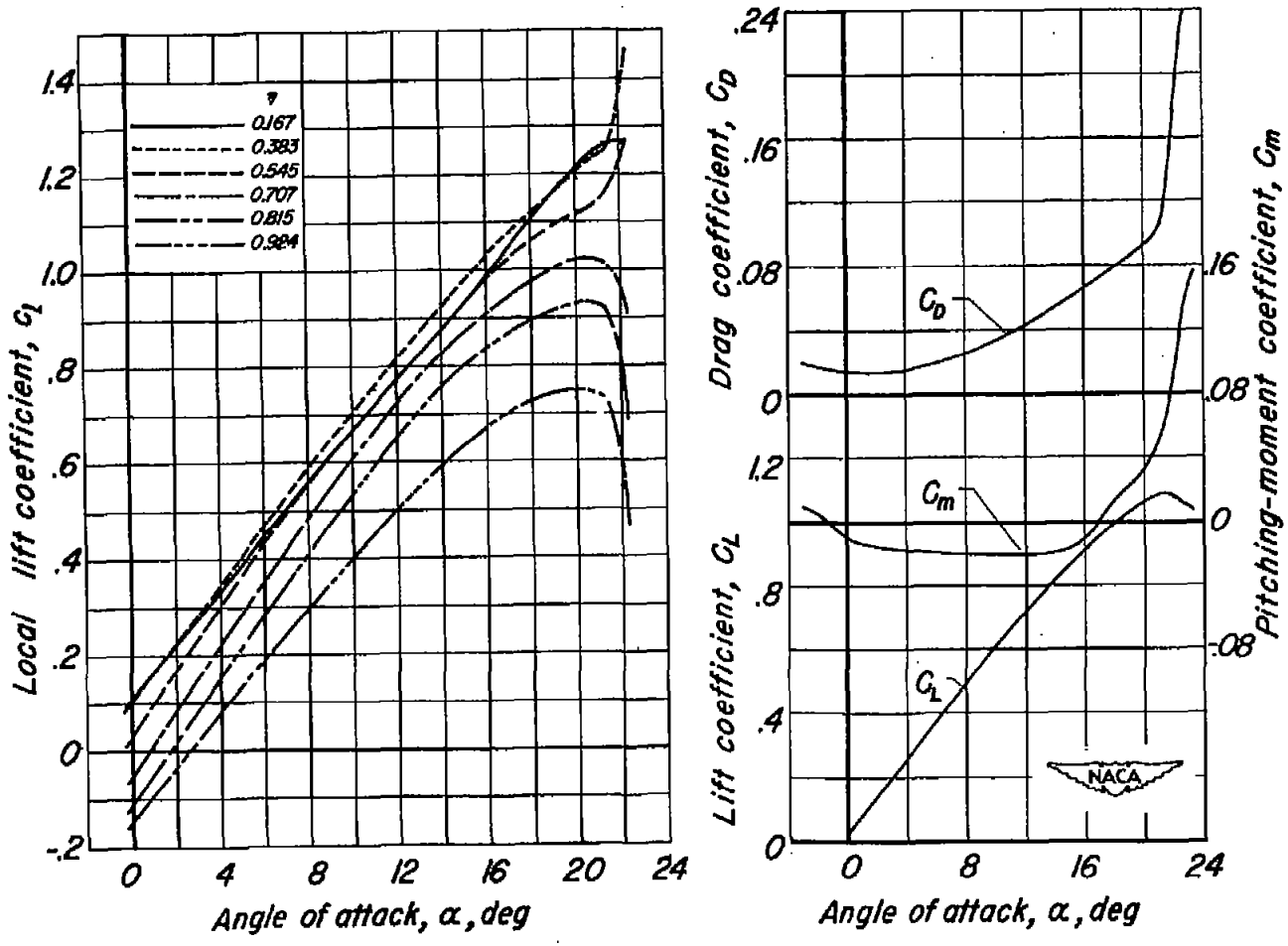

(b) Cambered, twisted wing.

Figure 6.—Concluded.

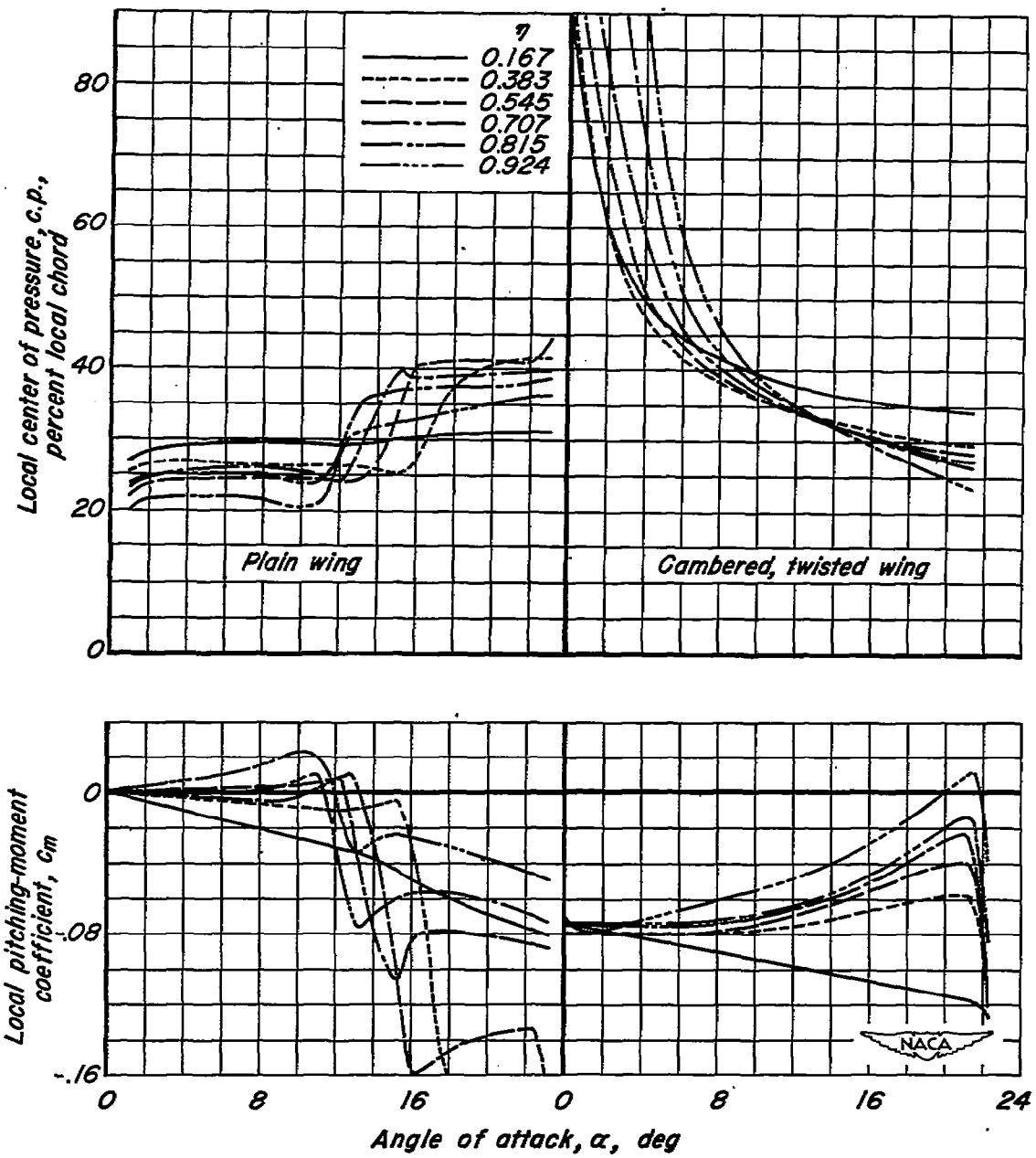

Figure 7.—Variation of local center of pressure and local pitching-moment coefficient with angle of attack.

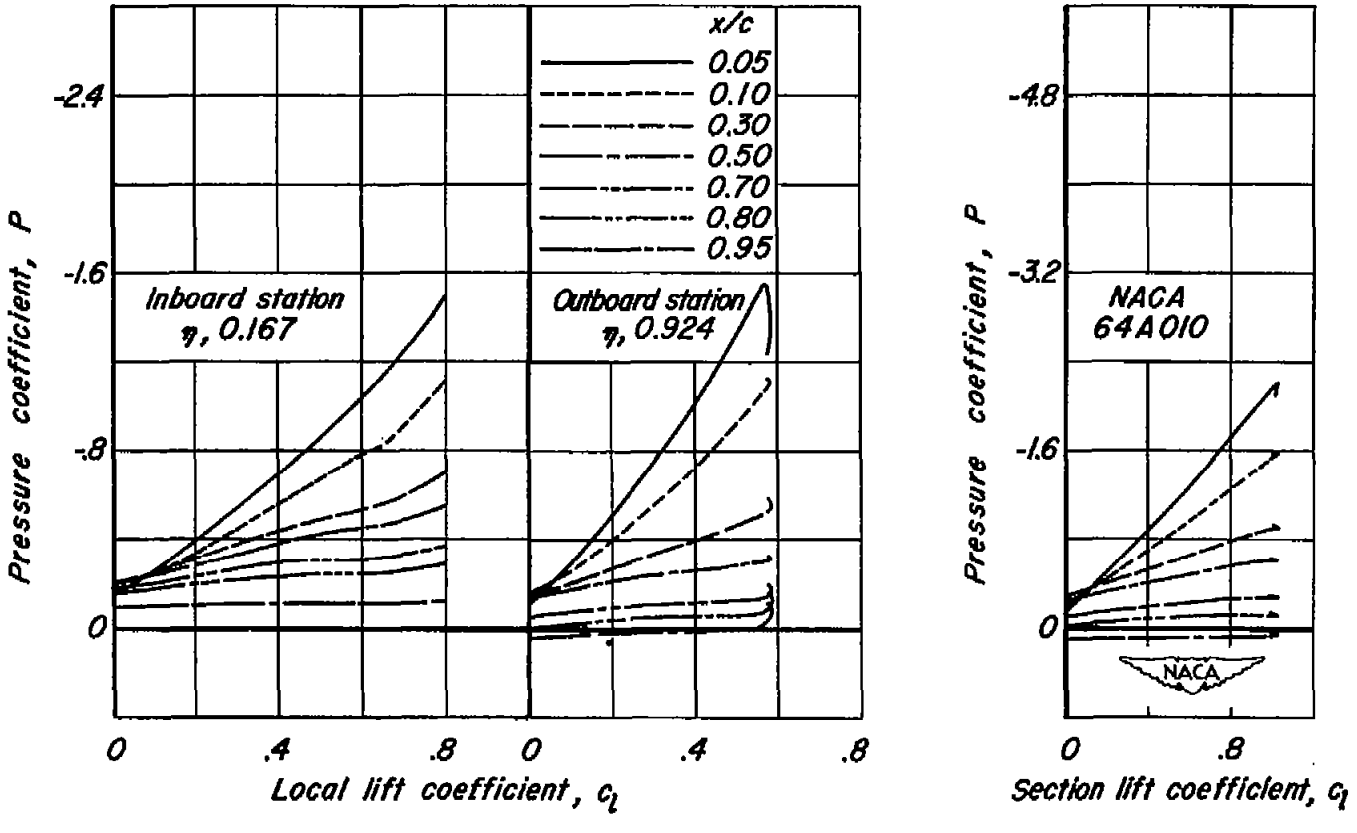

(a) Plain wing.

Figure 8.- Variation of the pressure coefficient with lift coefficient at several percent-chord points for an inboard station, an outboard station, and a two-dimensional section.

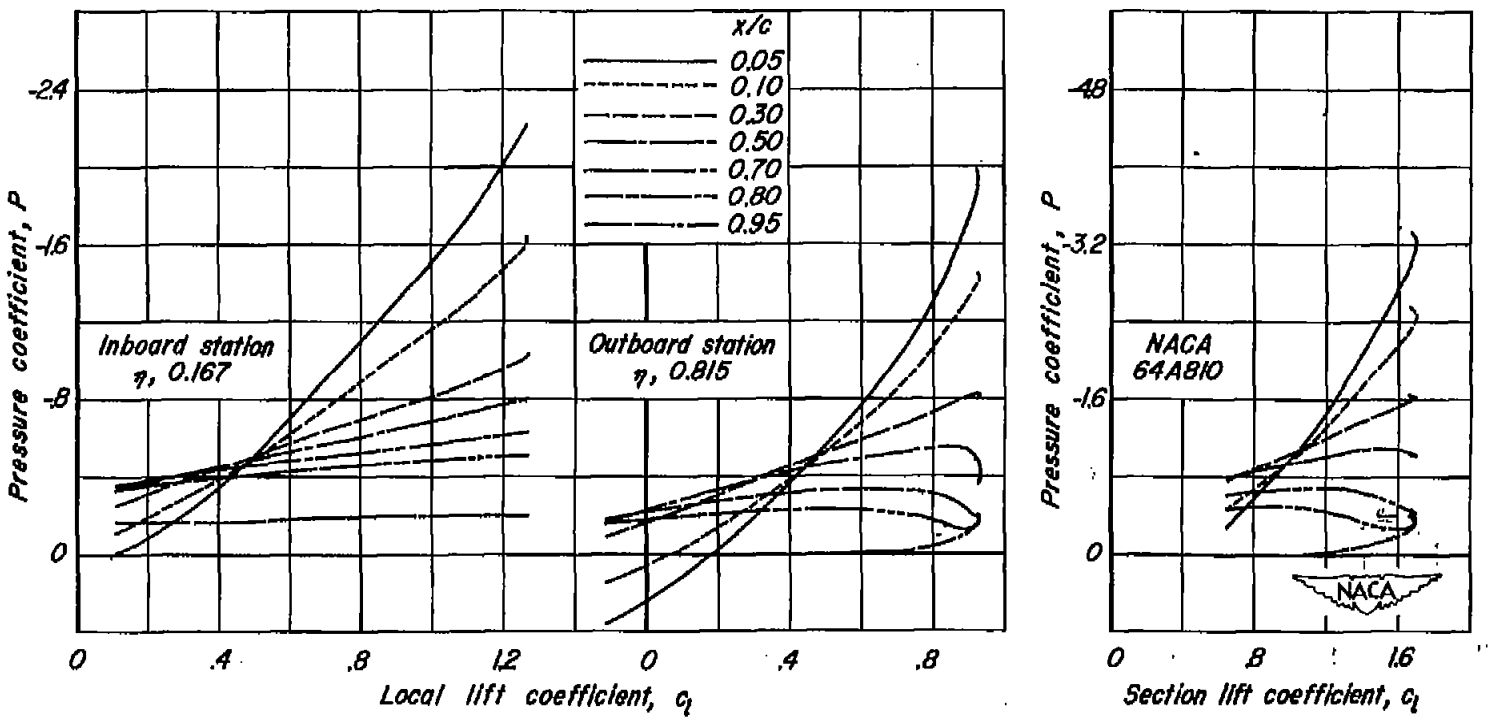

(b) Cambered, twisted wing.

Figure 8.– Concluded.

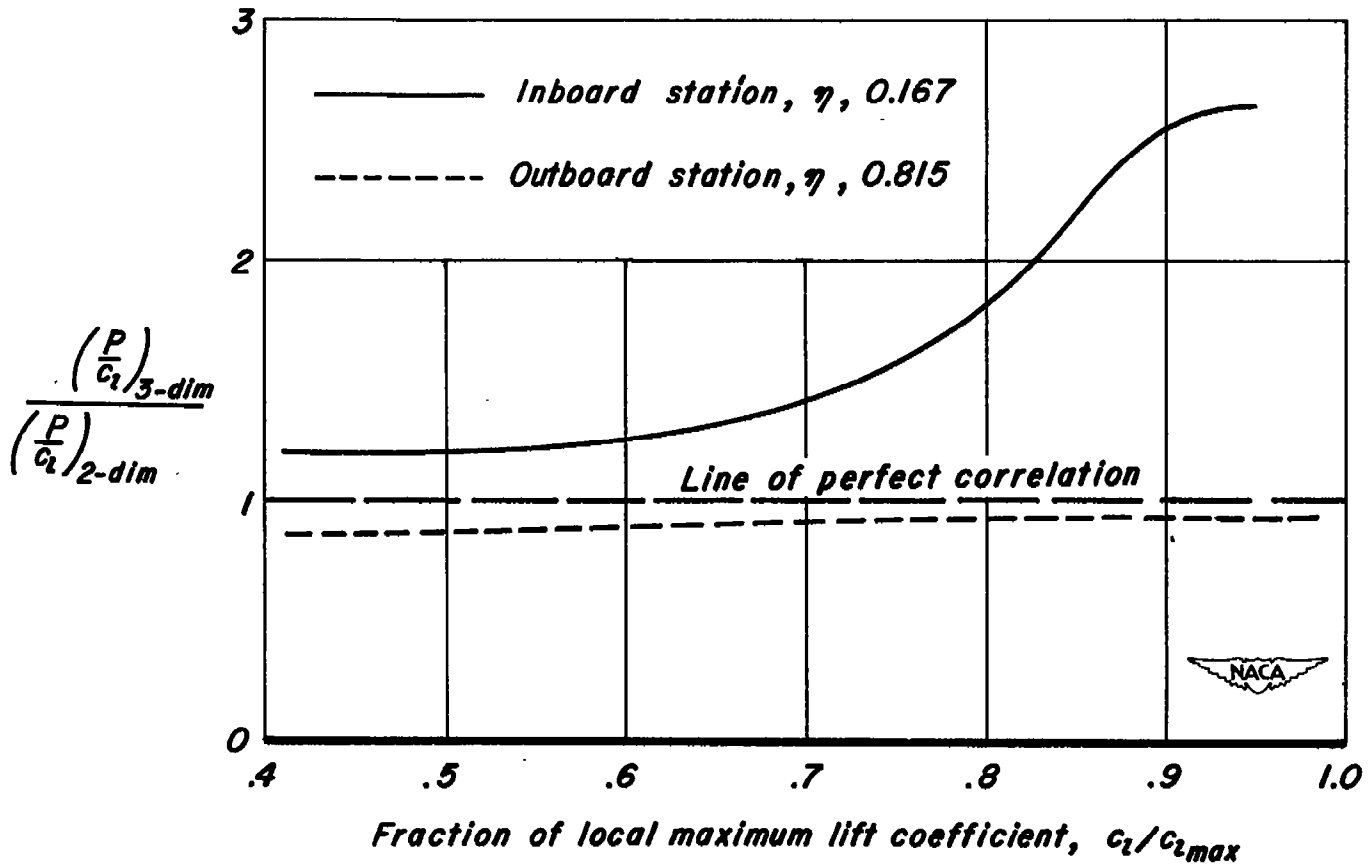

Figure 9.—The ratio of pressure coefficient on the cambered, twisted wing to pressure coefficient on the NACA 64A810 section at the 0.8-chord point for an inboard station and an outboard station.

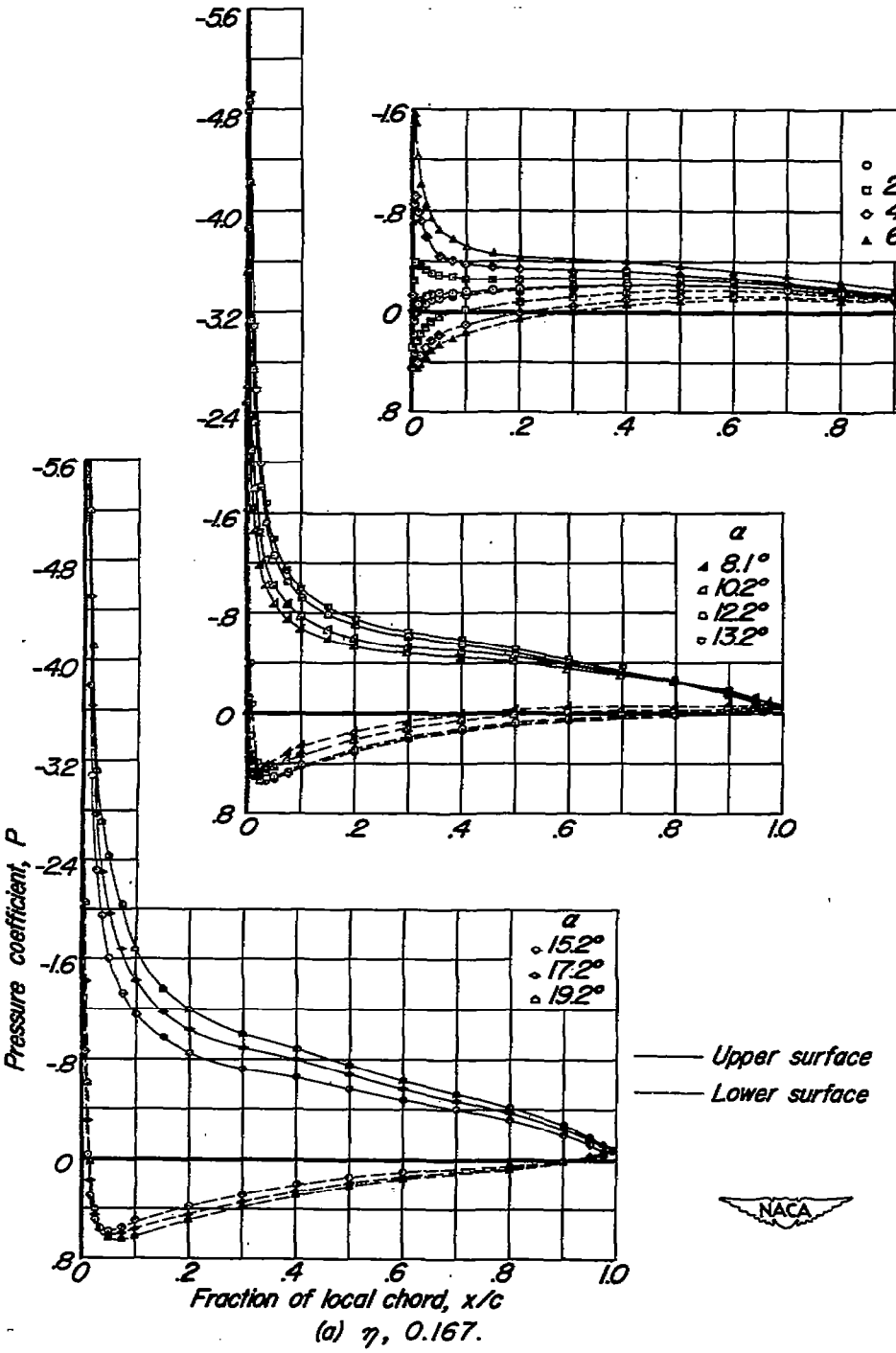

(a) η, 0.167.

Figure 10.– Pressure distribution on the plain wing. R, 8.0 million.

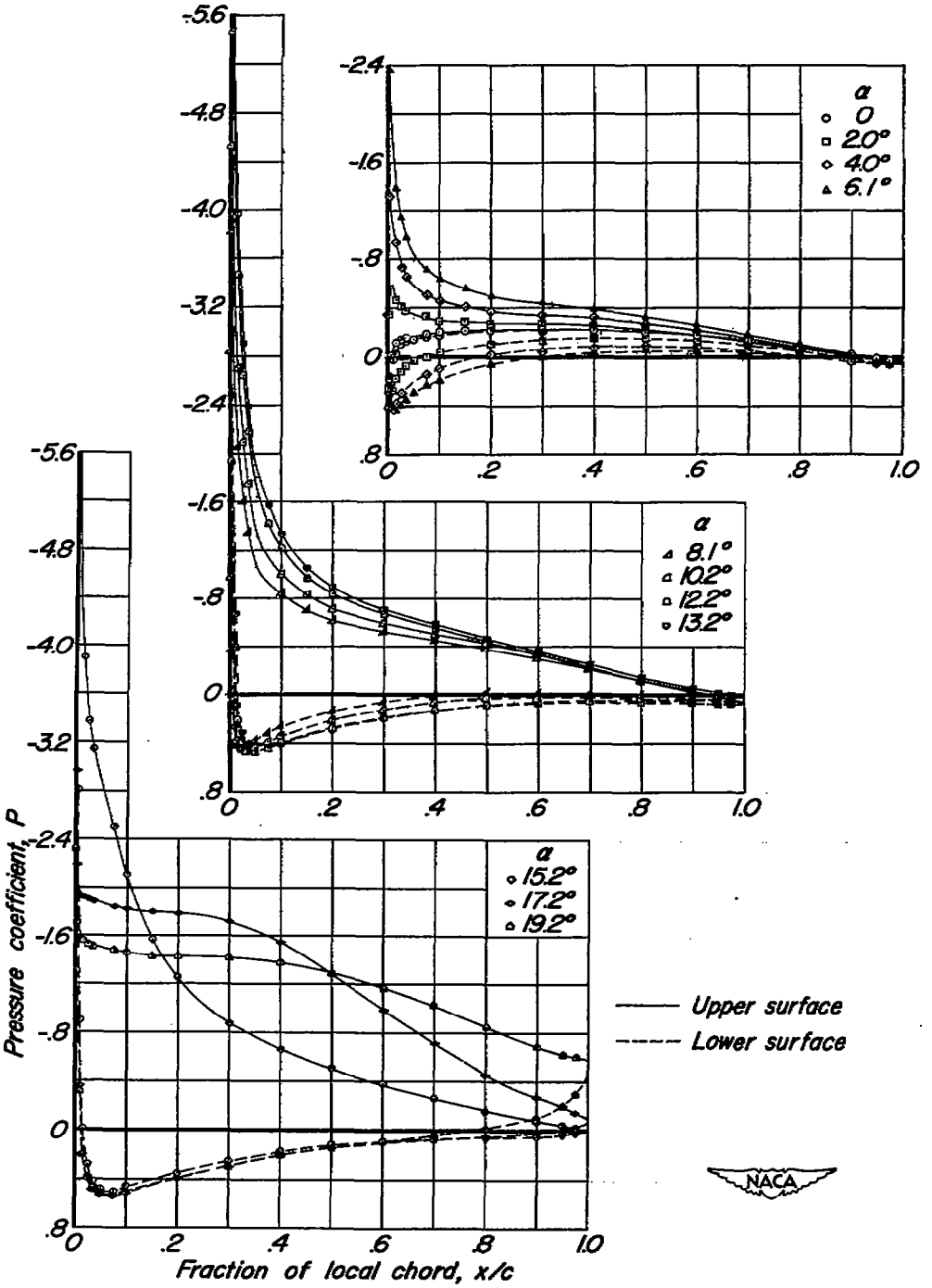

(b) η, 0.383.

Figure 10.–Continued.

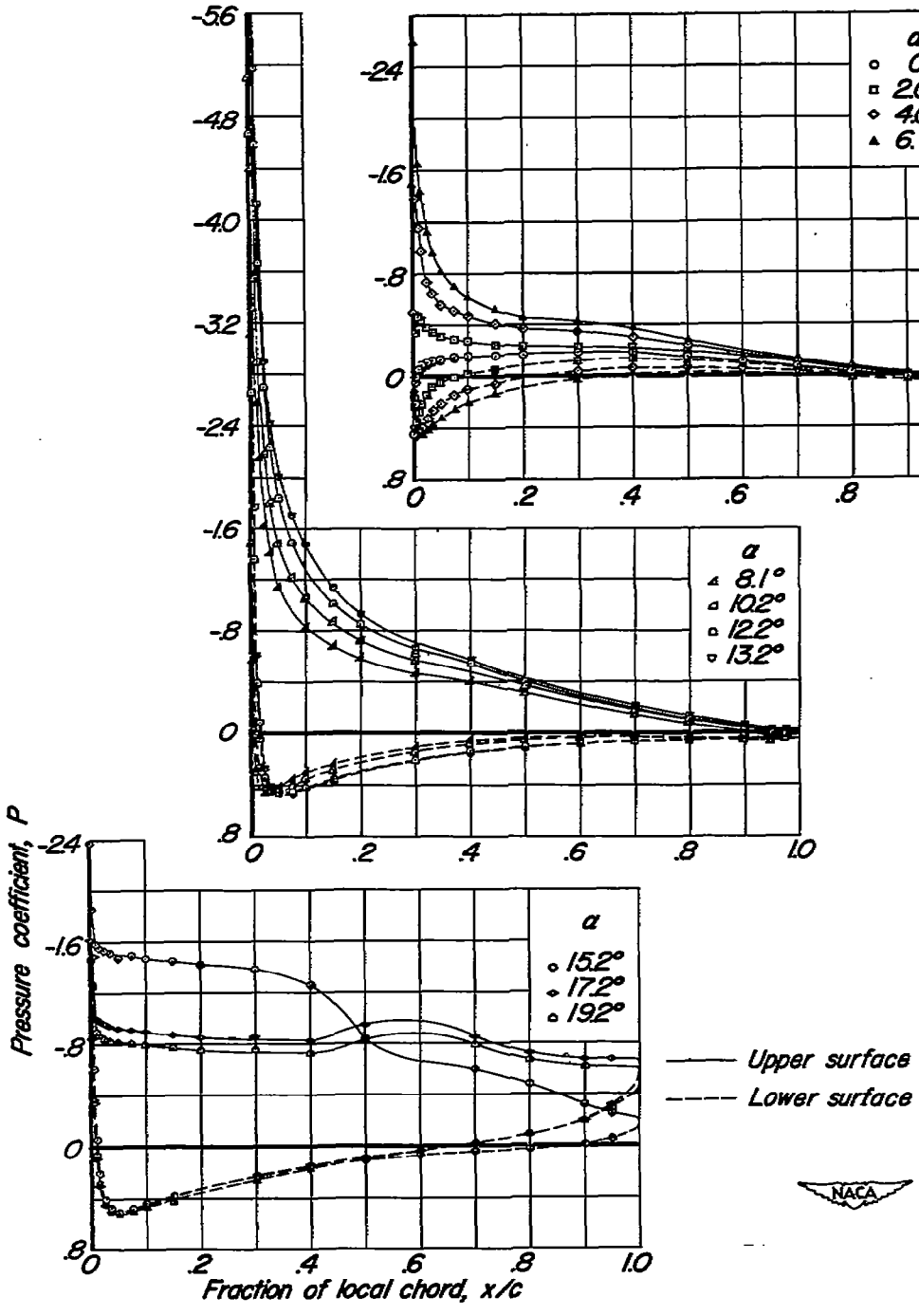

(c) η, 0.545.

Figure 10.—Continued.

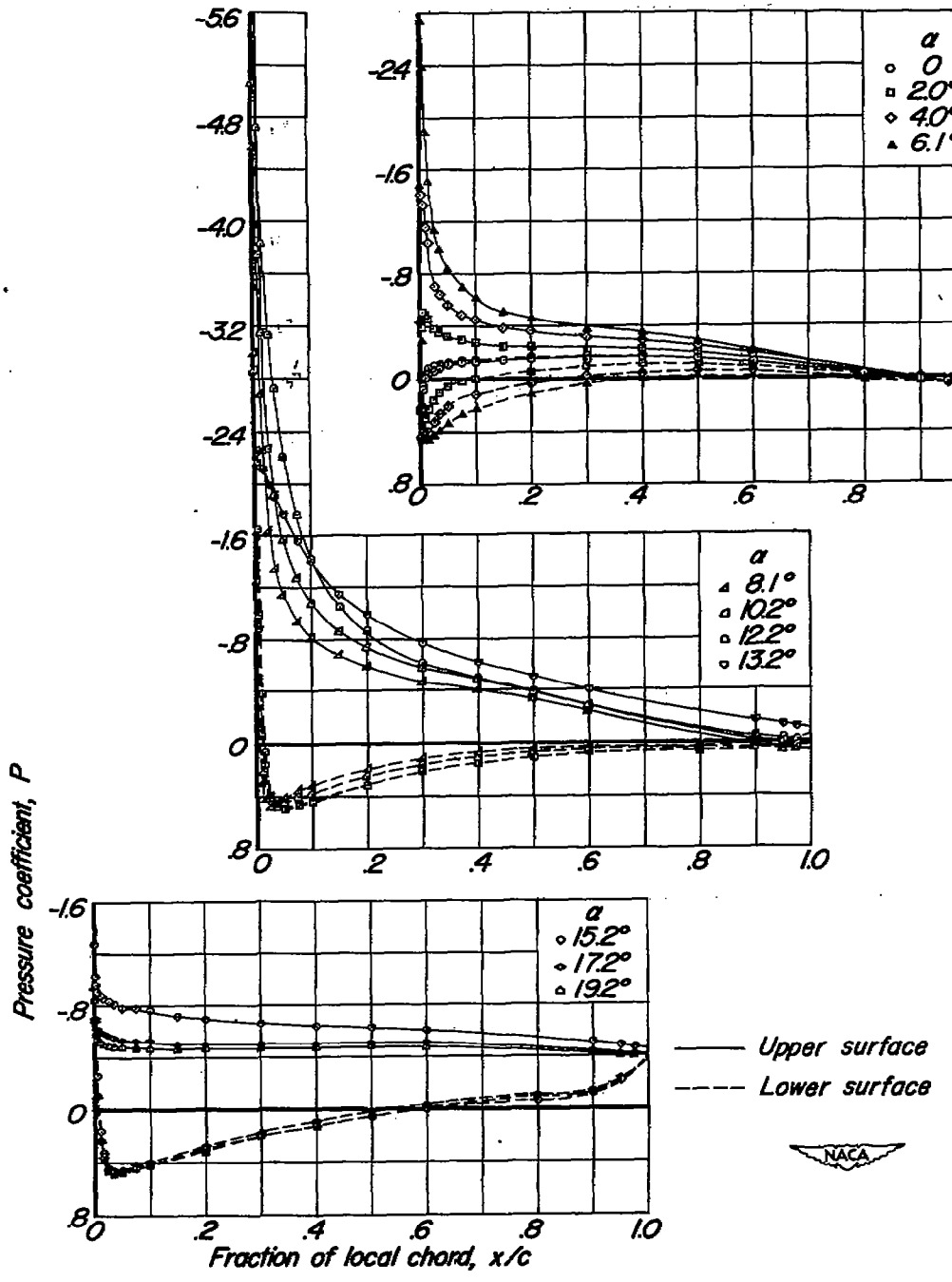

(d) η, 0.707.

Figure 10.—Continued.

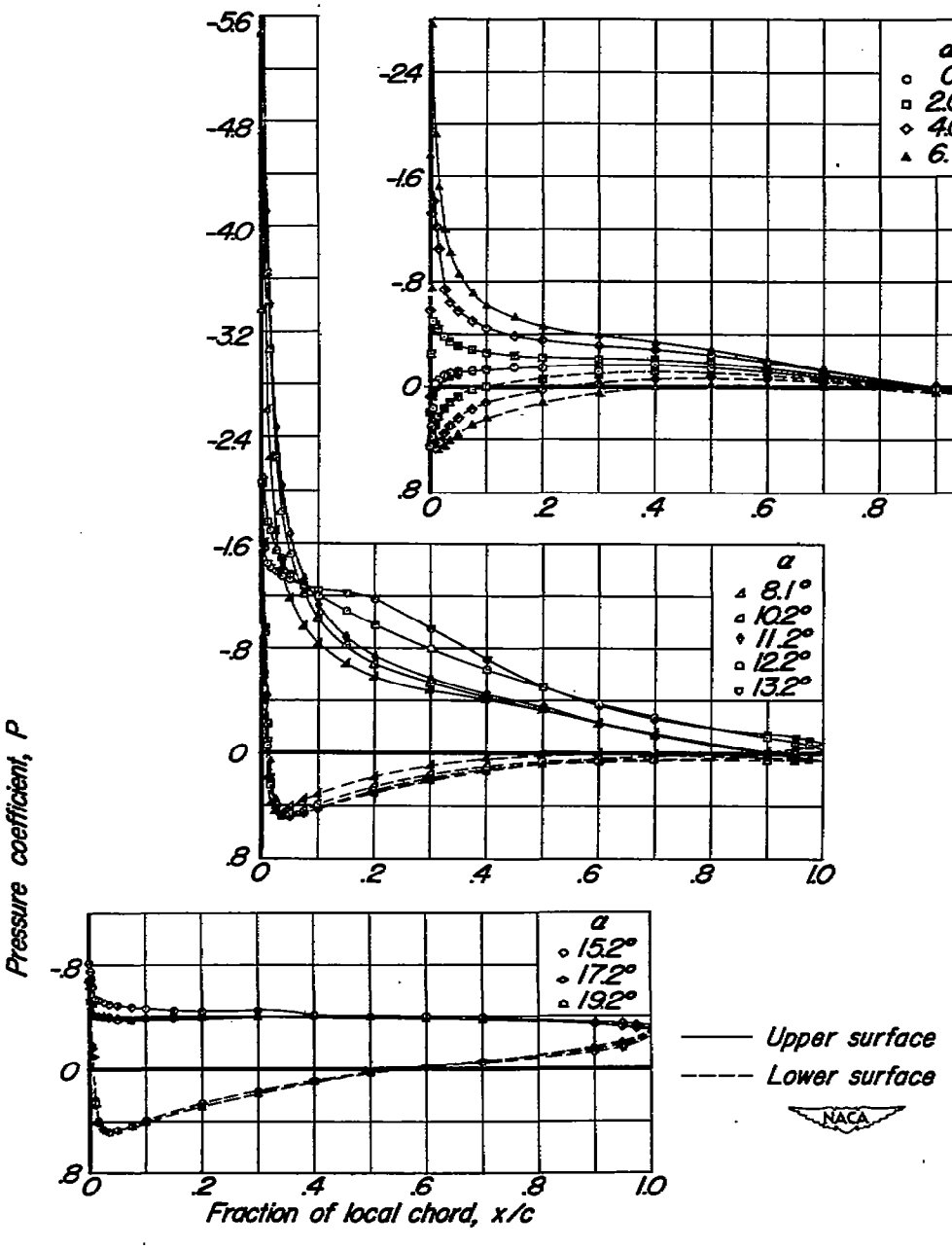

(e) η, 0.815.

Figure 10.–Continued.

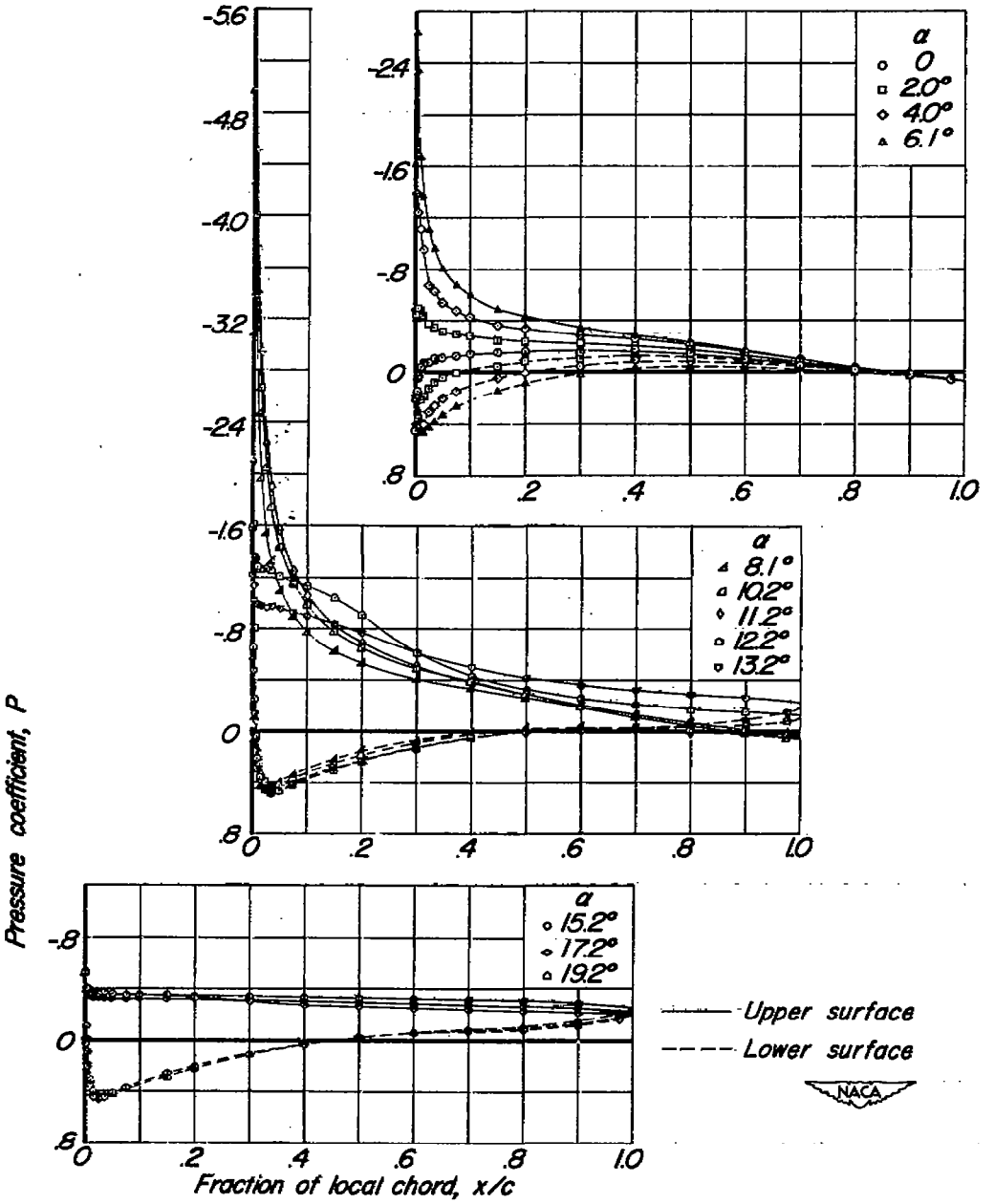

(f) η, 0.924.

Figure 10.–Concluded.

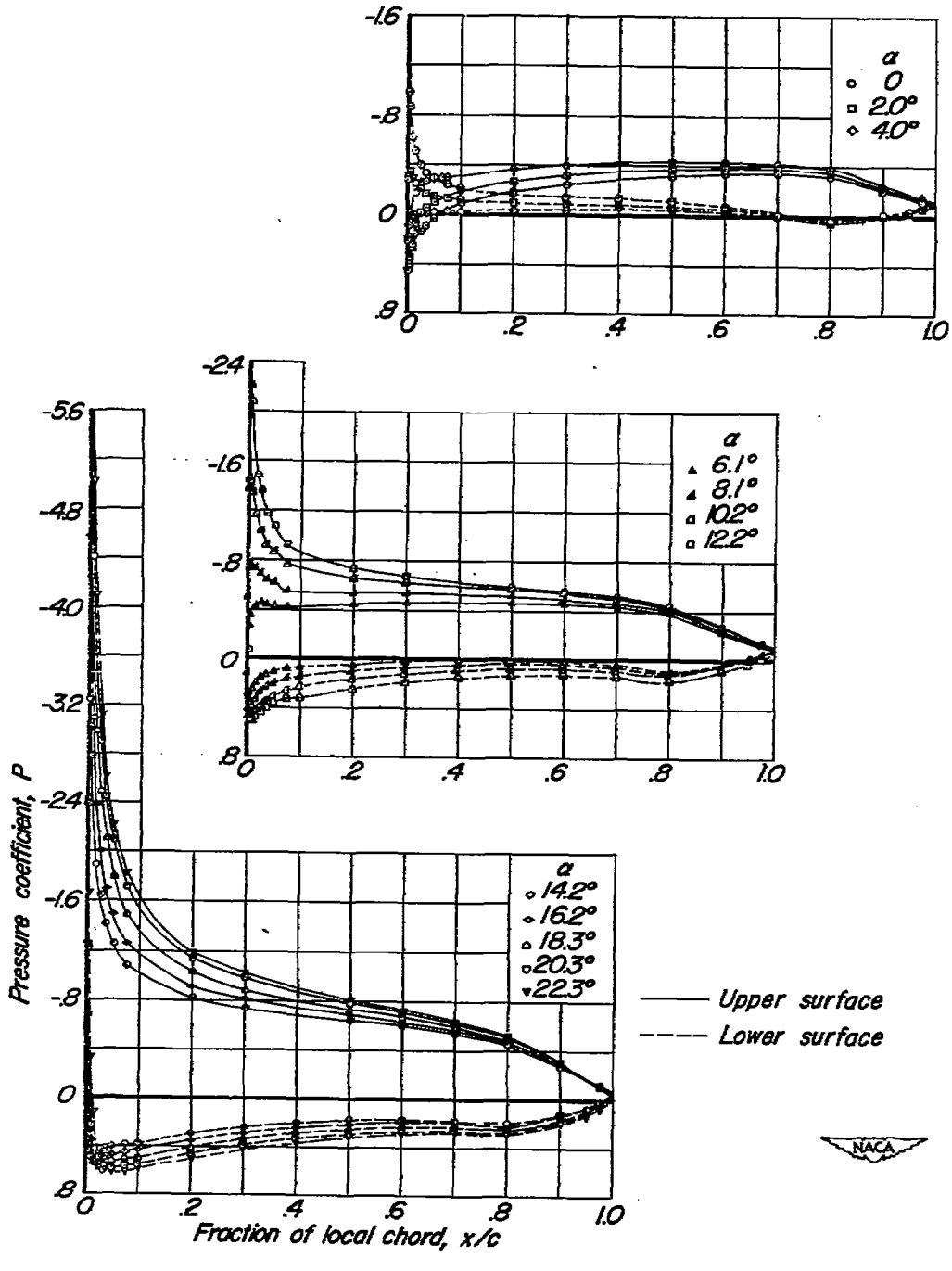

(a) η, 0.167.

Figure 11.–Pressure distribution on the cambered, twisted wing. R, 8.0 million.

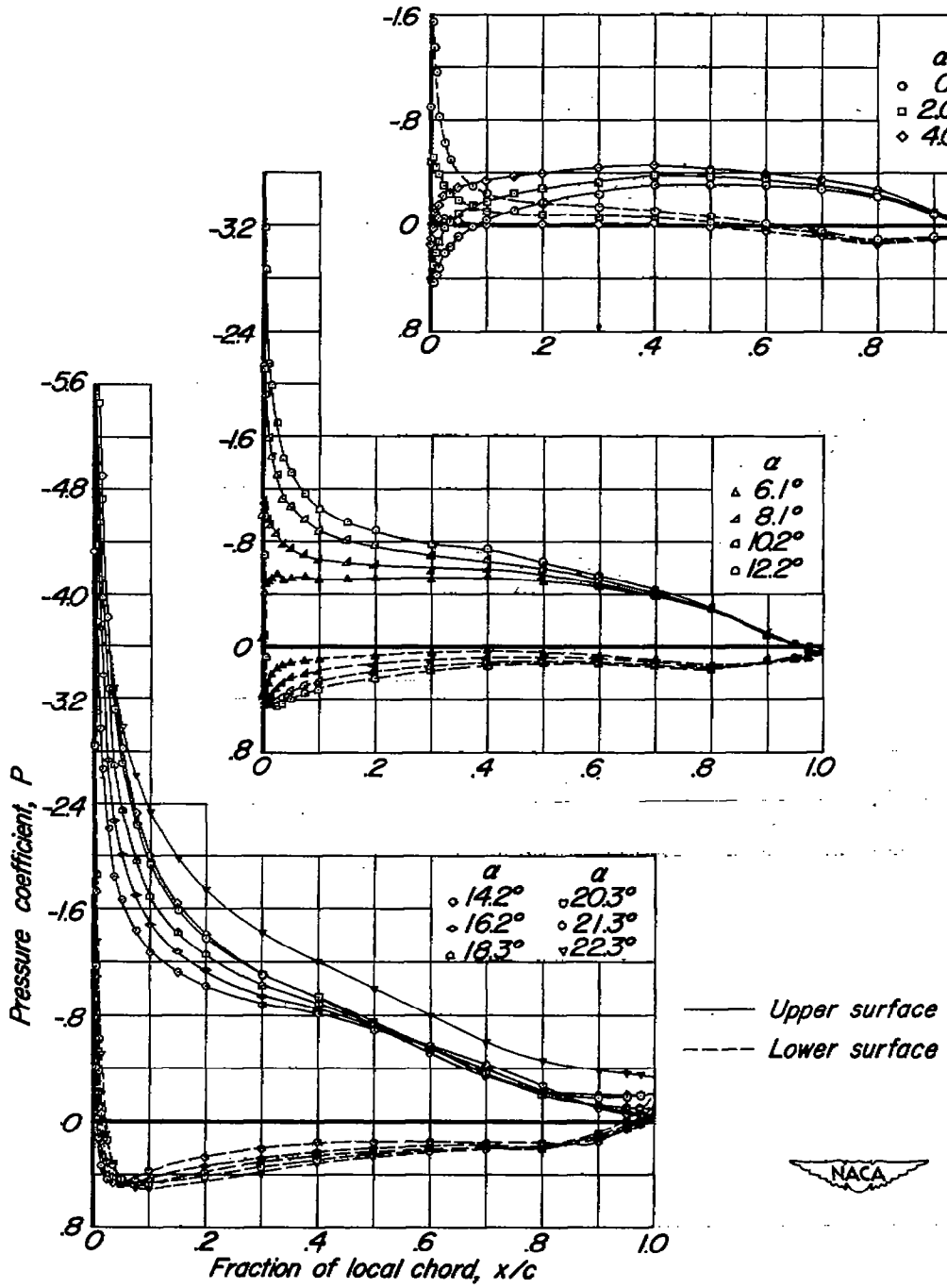

(b) η, 0.383.

Figure 11.—Continued.

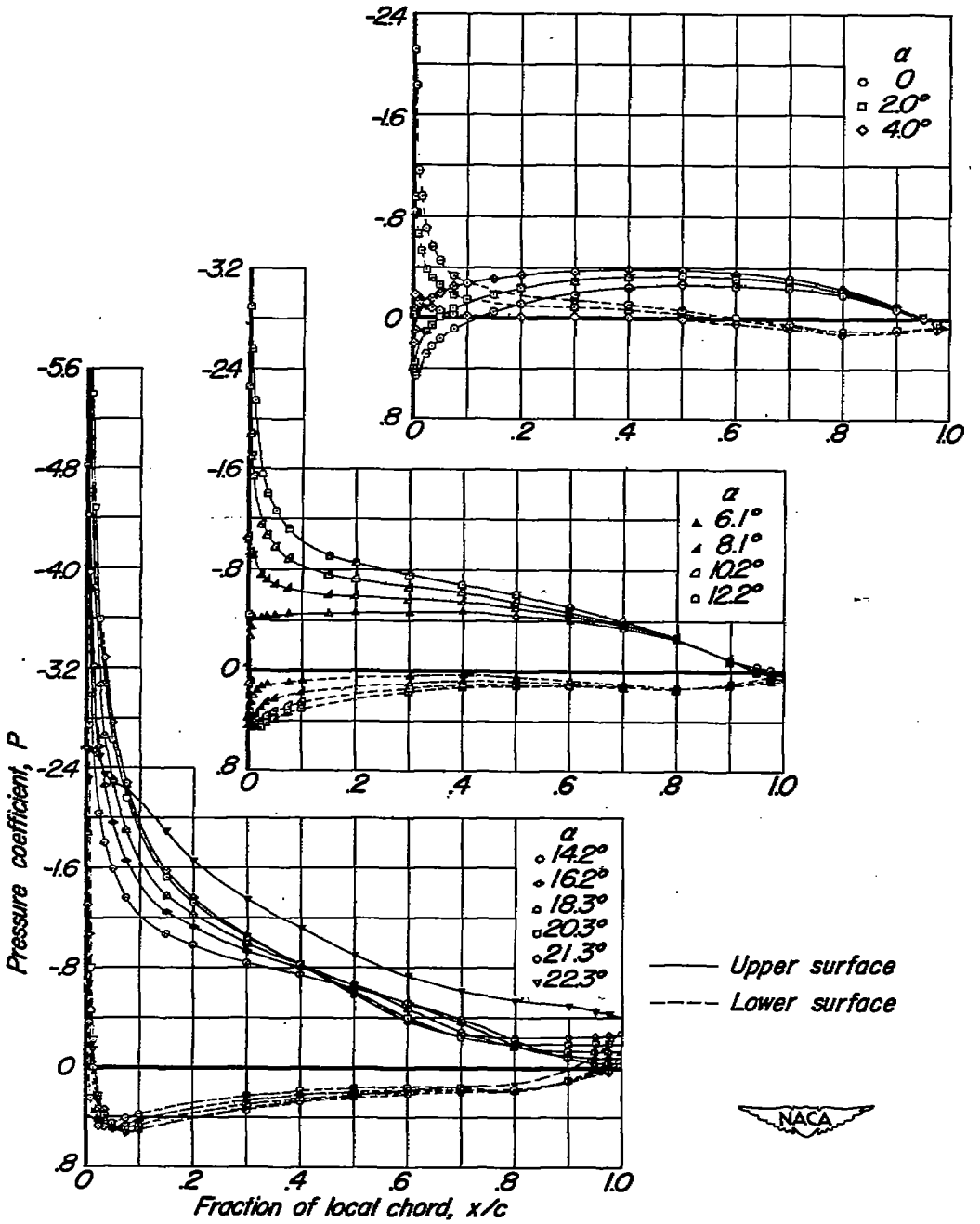

(c) η, 0.545.

Figure 11.–Continued.

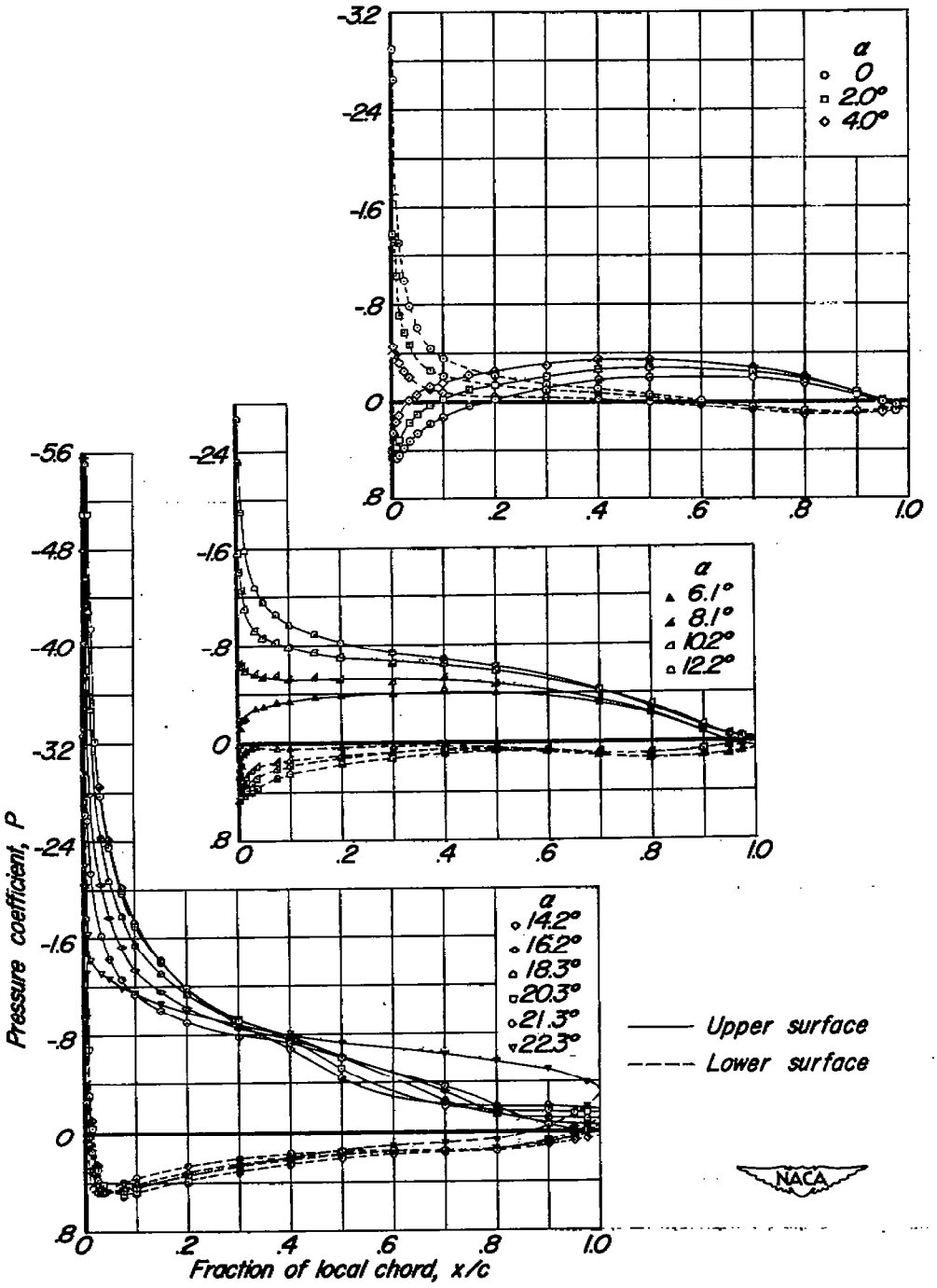

(d) η, 0.707.

Figure 11.–Continued.

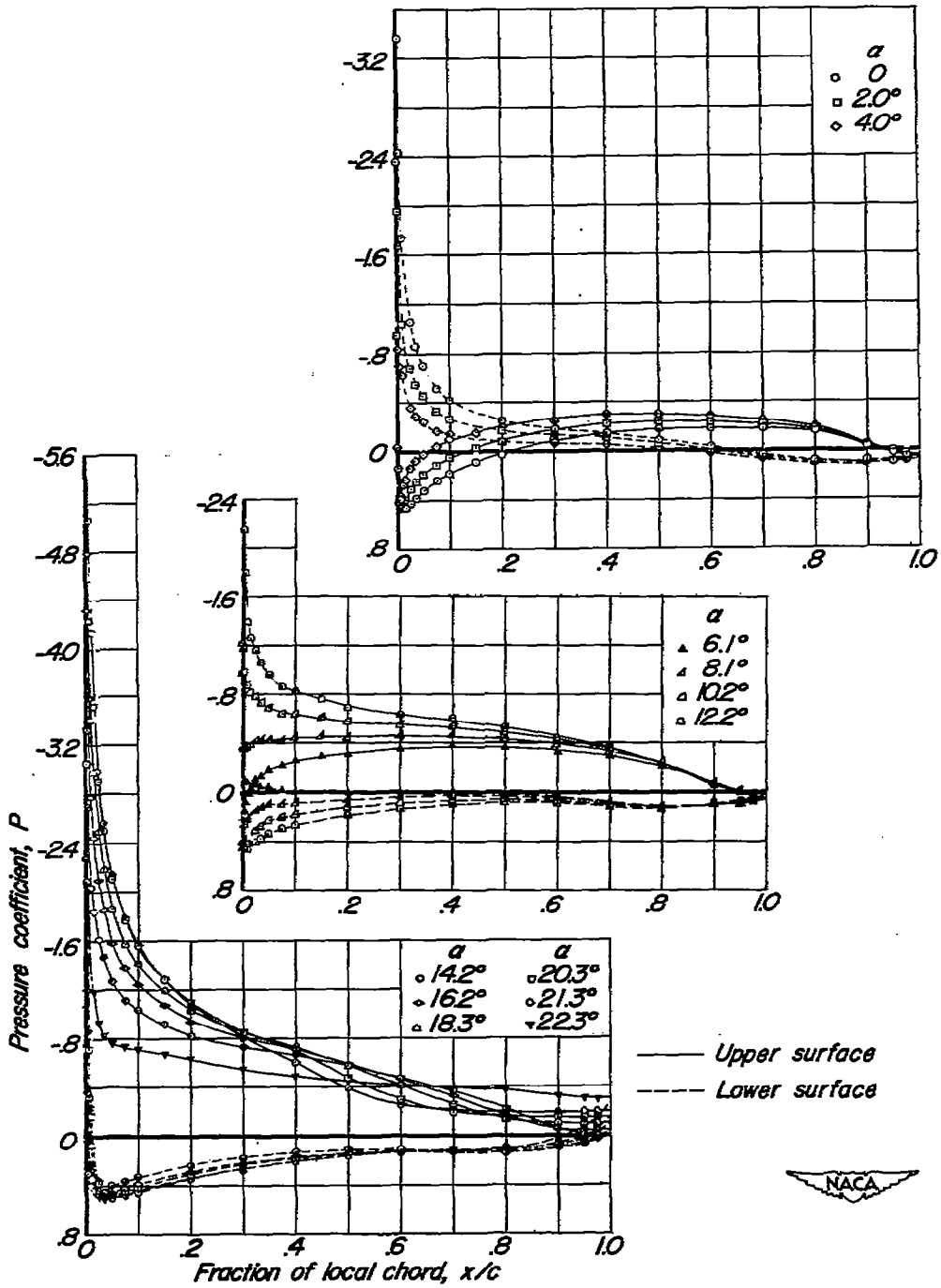

(e) η, 0.815.

Figure 11.—Continued.

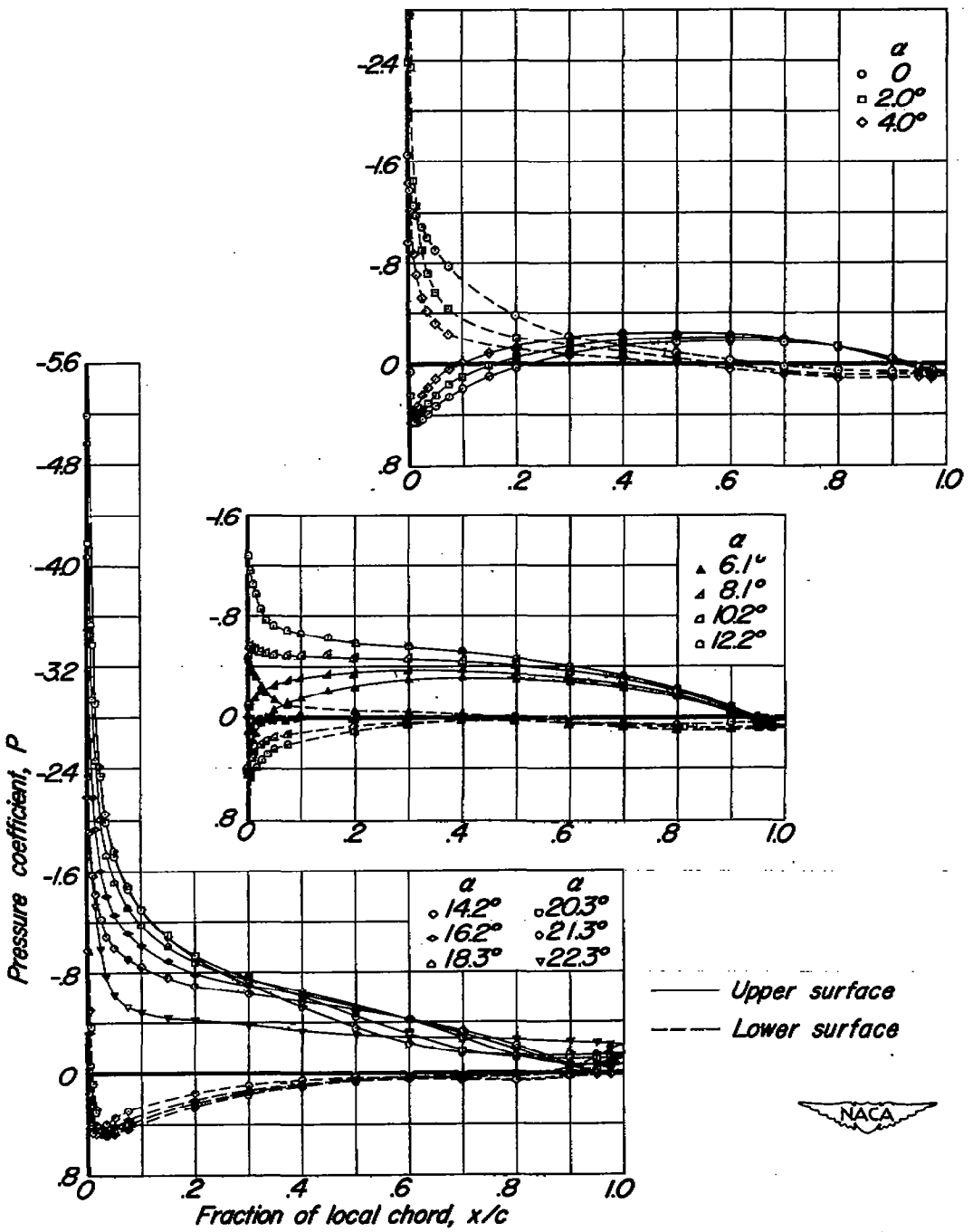

(f) η, 0.924.

Figure 11.–Concluded.